Ultradian rhythms in shell composition of photosymbiotic and non-photosymbiotic mollusks

Niels J. de Winter[1,2], Daniel Killam[3], Lukas Fröhlich[4], Lennart de Nooijer[5], Wim Boer[5], Bernd R. Schöne[4], Julien Thébault[6], Gert-Jan Reichart[5,7]

Affiliations

[1]Dept. of Earth Sciences, Vrije Universiteit Amsterdam, Amsterdam, the Netherlands

[2]Analytical, Environmental and Geochemistry group (AMGC), Vrije Universiteit Brussel, Brussels, Belgium

[3] San Francisco Estuary Institute, Richmond, CA, USA

[4] Institute of Geosciences, University of Mainz, Germany

[5] Dept. of Ocean Systems, Royal Netherlands Institute for Sea Research (NIOZ), Texel, the Netherlands

[6]Univ Brest, CNRS, IRD, Ifremer, LEMAR, 29280 Plouzané, France, (ORCID: 0000-0002-3111-4428)

[7]Dept. of Earth Sciences, Utrecht University, Utrecht, the Netherlands

Corresponding author: N.J. de Winter, n.j.de.winter@vu.nl

Abstract

The chemical composition of mollusk shells is a useful tool in (paleo)climatology since it captures inter- and intra-annual variability in environmental conditions. Trace element and stable isotope analysis with improved sampling resolution now allows *in-situ* determination of the composition of mollusk shell volumes precipitated at daily to sub-daily time intervals. Here, we discuss hourly resolved Mg/Ca, Mn/Ca, Sr/Ca and Ba/Ca profiles measured by laser ablation ICP-MS through shells of photosymbiotic giant clams (*Tridacna maxima*, *T. squamosa* and *T. squamosina*) and the non-photosymbiotic scallop *Pecten maximus*. Precise sclerochronological age models and spectral analysis allowed us to extract daily and tidal rhythms in the trace element composition of these shells. We find weak but statistically significant expressions of these periods and conclude that this cyclicity explains less than 10 % of the sub-annual variance in trace element profiles. Tidal and diurnal rhythms explain variability of at most 0.2 mmol mol^{-1} (~10 % of mean value) in Mg/Ca and Sr/Ca, while ultradian Mn/Ca and Ba/Ca cyclicity has a median amplitude of less than 2 µmol mol^{-1} mol mol^{-1}(~ 40 % and 80 % of the mean of Mn/Ca and Ba/Ca, respectively). Daily periodicity in Sr/Ca and Ba/Ca is stronger in *Tridacna* than in *Pecten*, with *Pecten* showing stronger tidal periodicity. One *T. squamosa* specimen which grew under a sunshade exhibits among the strongest diurnal cyclicity. Daily cycles in trace element composition of giant clams are therefore unlikely to be driven by variations in direct insolation, but rather reflect an inherent biological rhythmic process affecting element incorporation. Finally, the large amount of short-term trace element variability unexplained by tidal and daily rhythms highlights the dominance of aperiodic processes in mollusk physiology and/or environmental conditions on shell composition at the sub-daily scale. Future studies should aim to investigate whether this remaining variability in shell chemistry reliably records weather patterns or circulation changes in the animals' environment.

1. Introduction

Patterns in growth increments, microstructure, and chemical composition of accretionary carbonate bioarchives yield detailed information about the environmental conditions and biological rhythm of carbonate producing animals (Dunbar and Wellington, 1981; Jones, 1983; Witbaard et al., 1994; Klein et al., 1996; Surge et al., 2001; Schöne et al., 2005a; Ivany, 2012; Schöne and Gillikin, 2013; DeCarlo and Cohen, 2017; Killam and Clapham, 2018a). These characteristics have spurred the development of a multitude of techniques for extracting information about life history (Jones and Quitmyer, 1996; Schöne et al., 2005b; Eggins et al., 2003; Anand and Elderfield, 2005; Goodwin et al., 2009; Mahé et al., 2010; Comboul et al., 2014; DeCarlo and Cohen, 2017; Judd et al., 2018; Winter et al., 2022), carbonate chemistry (Sinclair et al., 1998; Lazareth et al., 2003; Schöne et al., 2010; de Winter and Claeys, 2017; Warter and Müller, 2017; Huyghe et al., 2021; de Winter et al., 2021b) and microstructure (Lazier et al., 1999; Checa et al., 2007; Popov, 2014; Gilbert et al., 2017; Crippa et al., 2020; Höche et al., 2020, 2021; Wichern et al., 2022) from carbonate shells and skeletons. As a result, (fossil) carbonate skeletons have gained much attention as archives of past environmental and climate change (Lough, 2010; Schöne and Gillikin, 2013; Ivany and Judd, 2022 and references therein).

Three characteristics make the shells of marine mollusks especially valuable as climate archives: (1) Nearly all marine mollusks precipitate their shells in equilibrium with the stable oxygen isotope composition of ambient sea water, except for juvenile oysters, some mollusks growing near hydrothermal vents and some deep-burrowing species (Schöne et al., 2004; Hallmann et al., 2008; Wisshak et al., 2009; Huyghe et al., 2021; de Winter et al., 2022), (2) mollusk shells have a high fossilization potential and long geological history, dating back to the beginning of the Phanerozoic (Al-Aasm and Veizer, 1986a, b; Jablonski et al., 2003; Cochran et al., 2010; Jablonski et al., 2017; de Winter et al., 2017, 2018; Coimbra et al., 2020), (3) the incremental growth of mollusk shells allows internal dating within the shell, yielding chronologies of shell

growth with sub-annual precision (Richardson et al., 1980; Jones, 1983; Schöne et al., 2005b; Goodwin et al., 2009; Huyghe et al., 2019). These advantages enable mollusk shells to record important information about climate and ambient water chemistry on the seasonal scale. Thereby, reconstructions from mollusk shells are highly complementary to other, less highly resolved but longer-term, climate and environmental reconstructions like sedimentary records, tree rings and ice cores (Black, 2009; Bougeois et al., 2014; Petersen et al., 2016; Tierney et al., 2020; de Winter et al., 2021a).

The resolution of the mollusk shell archive is not limited to seasonal variability. Studies monitoring the behavior of mollusks during growth experiments show that their activity varies as a function of environmental conditions (e.g., temperature and food availability) and follows ultradian rhythms which may contain daily to hourly periodicities, probably linked to diurnal and tidal cycles, or lack periodic behavior altogether (Rodland et al., 2006; García-March et al., 2008; Tran et al., 2011; Ballesta-Artero et al., 2017; Xing et al., 2019; Tran et al., 2020). Analyses of growth patterns and, more recently, composition of shell carbonate deposited at these short time intervals show that these ultradian rhythms can be recorded in mollusk shells (Pannella, 1976; Richardson et al., 1980; Sano et al., 2012; Warter et al., 2018; de Winter et al., 2020). This raises the question whether mollusk shells reliably record behavioral changes, high frequency (paleo-)weather or circulation patterns (e.g. Komagoe et al., 2018; Yan et al., 2020; Poitevin et al., 2020). Alternatively, the presence of daily cyclicity in shell chemistry may yield information about the paleobiology of extinct mollusks, such as the use of photosymbiosis (e.g. Sano et al., 2012; Warter et al., 2018; de Winter et al., 2020). The latter seems plausible given the effect of photosymbiosis on shell mineralization in modern tridacnids (Ip and Chew, 2021) and on the trace element composition of aragonite in modern photosymbiotic scleractinian corals (Cohen et al., 2002; Meibom et al., 2003; Inoue et al., 2018). If proven true, daily variability in bivalve shells may serve as a proxy for photosymbiosis in the fossil record (e.g. de Winter et al., 2020). This is of interest

because photosymbiosis is a derived adaptation of some tropical bivalve species (e.g., tridacnids) and its prevalence in the fossil record has important implications for the ecological niche of fossil mollusks (e.g. Vermeij, 2013). In addition, photosymbiosis can affect mollusk shell composition, and understanding it is therefore critical for the interpretation of chemical proxies in mollusk shells for environmental reconstructions (Killam et al., 2020). Finally, improving our understanding of photosymbiosis in tropical ecosystems sheds light on the resilience of photosymbiotic organisms to environmental change, now and in the geological past. The latter is of special interest in light of the ongoing climate and biodiversity crises, which are profoundly affecting these sensitive ecosystems (Pandolfi and Kiessling, 2014).

In this study, we investigate shell growth patterns and shell chemistry of the photosymbiotic bivalves *Tridacna maxima*, *T. squamosa* and *T. squamosina* as well as the non-photosymbiotic scallop *Pecten maximus*. *P. maximus* was chosen as a non-photosymbiotic counterpart in comparison with the tridacnids because of its comparatively high growth rate and the presence of daily striae visible on the outer surface of its shell, which make it possible to construct accurate shell chronologies (Chauvaud et al., 2005). We combine ultra-high-resolution (micrometer-scale) Mg/Ca, Sr/Ca, Mn/Ca and Ba/Ca measurements in the shells with detailed sclerochronology to investigate the variability in these trace elements over time in all four species. The aims of this study are to investigate (1) whether the shells record high-frequency variability in shell chemistry that can be linked to environmental and/or circadian rhythms and (2) whether the presence of photosymbiosis influences the expression of this variability in the shell composition.

2. Materials and methods

2.1 Preparation of *P. maximus* specimens

Three specimens of the King scallop *P. maximus* (labeled "**PM2**", "**PM3**" and "**PM4**") were collected alive on 15/11/2019 on the southern coast of the Bay of Brest near Lanvéoc, France (48°17′N 4°30′W) with permit from the Prefect of the Brittany Region by SCUBA divers at a depth of approximately 8 m (see Fröhlich et al., 2022); **Figure 1**). Note that water depth in the Bay of Brest varies significantly due to the macrotidal regime with a mean tidal range of 2.8 – 5.9 m with extreme ranges up to 7.2 m (Guillaume Olivier et al., 2021; Service Hydrographique et Océanographique de la Marine - Géoportail, 2022). Collected specimens contained at least one full year of growth based on the visibility of one winter growth line on the outside of the shell (age class 1; see Thébault et al., 2022; **Fig 1F** and **S1**). Specimens were frozen at -20°C immediately after collection. Soft body parts and epibionts were removed from the shells before further treatment. Shells were superficially cleaned using a plastic brush and adhering sediment was removed by ultrasonication in deionized water. The flat, left valves were used for elemental and sclerochronological analysis following previous studies on *P. maximus* (Thébault et al., 2022; Fröhlich et al., 2022).

High-resolution color photos were made of the outside of the left valve of the shell using a mirror-reflex camera (Canon EOS 600 DSLR camera connected to a Wild Heerbrugg binocular microscope equipped with a Schott VisiLED MC 1000 sectoral dark-field light source) aimed downward perpendicular to the working surface. Overlapping images of the shells were stitched together using Image Composite Editor v2.0.3.0 (Microsoft Research Computational Photography Group, Redmond, WA, USA). The stitched images were used to count and measure daily striae on the shell surface (see **Fig. 1** and **S1**). To obtain a fully focused composite of the complete shell, dynamic focusing was applied to allow all parts of the slightly curved surface of the shell to

140 come into focus. Dynamic focus images where later stitched together using focus stacking in
141 Helicon Focus (Helicon Focus 7.7.5; HeliconSoft, Kharkiv, Ukraine; see **S1**).

142 Cross sections were cut through all three *P. maximus* shells perpendicular to the daily growth
143 lines (striae) from the ventral margin of the shell to the shell hinge (see **Fig. 1B-D** and **S1**) along
144 the axis of maximal growth. Shells were fortified with a protective layer of metal epoxy (Gluetec
145 Wiko Epofix 05) before sectioning using a Buehler Isomet 1000 low-speed precision saw (Buehler
146 Inc, Lake Bluff, IL, USA) equipped with a diamond-coated wafering thin blade (0.4 mm thickness;
147 number 15LC 11–4255) at 200 rpm. Parallel cuts were made to allow shell sections to be glued
148 to glass plates for grinding (down to F1200 grit SiC powder) and high-grade polishing (1 µm Al_2O_3
149 suspension on Buhler polishing cloth, MasterTex). Two cross sections were made through
150 specimens **PM2** and **PM3**: One through a “rib” of the shell (i.e., radial segment that protrudes
151 away from the interior, named **PM2_1** and **PM3_1**) and one through a “valley” (i.e., radial segment
152 between two “ribs” that lies deeper towards the interior, named **PM2_2** and **PM3_2**; see **Fig. 1**
153 and **S1**). The dual sections were cut to compare shell chemistry between the “ribs” and “valleys”
154 of the shell. Specimen **PM4** was only sectioned once, through a “valley” in the shell, yielding a
155 total of five cross sections through the *P. maximus* specimens.

156

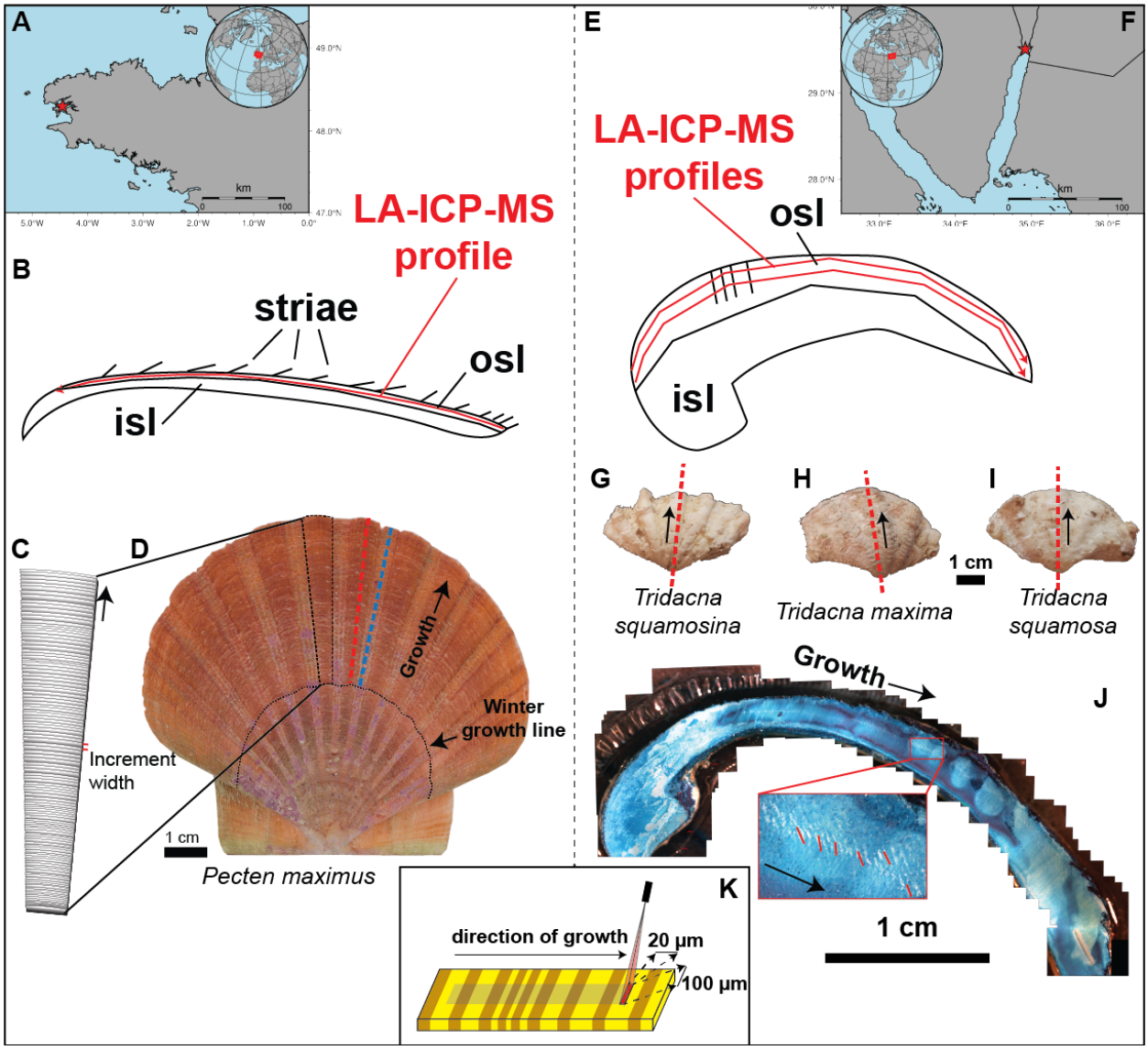

Figure 1: **Overview of sample locations and preparation steps**. **A)** Location of the Bay of Brest, with the red star indicating the sampling location. **B)** Schematic cross section through *P. maximus* showing how the LA-ICP-MS line scan (red line) was positioned within the outer shell layer (OSL).**C)** Schematic representation of a segment through the shell of *P. maximus* showing the striae which are deposited daily, and which were counted to establish age models (see also **B**). **D**) Left valve of *P. maximus* (**PM2**) used in this study, with dashed lines showing the position of cross sections through a rib (red) and valley (blue) in the shell. Black arrow indicates growth direction away from the shell hinge. The black dotted line highlights a winter growth stop. **E)**

Schematic cross section through a tridacnid, illustrating the positions of parallel LA-ICP-MS line scans (red lines) through these shells within the OSL. **F)** Position of the Gulf of Aqaba, with the red star indicating the sample location for tridacnids. **G-I)** Pictures of (from left to right) *T. squamosa* (specimen **TSFRS1**), *T. maxima* (specimen **TM29**) and *T. squamosina* (specimen **SQSA1**) with dashed red lines indicating the positions of the cross sections used for LA-ICP-MS analysis (see **C**) and black arrows indicating the direction of growth. **J**) Example of Mutvei-stained cross section through a *T. maxima* specimen used to visualize and count growth lines, with the insert showing part of the OSL where growth lines were counted (red lines) to establish age models for the tridacnids. Black arrows indicate the direction of growth. **K)** Schematic representation of the LA-ICP-MS line scanning setup with the rectangular spot size (100 * 20 µm; see **S11**) that was positioned parallel to the growth layers in the shell.

178 2.2 Preparation of *Tridacna* specimens

179 A total of 5 tridacnid specimens, two *T. maxima* (named **TM29** and **TM84**), two *T. squamosa*
180 (named **TS85** and **TSFRS1**) and one *T. squamosina* (**SQSA1**) specimen, were collected in the
181 summer of 2016 from beach death assemblages on the coast of the Gulf of Aqaba with permit
182 from the Israeli National Parks Authority (**Figure 1**; see details in Killam et al., 2020). One cultured
183 *Tridacna squamosa* shell (**TSM1**) was obtained from the National Center for Mariculture, Eilat.
184 Species were determined following shell characteristics of the local population as cited in Roa-
185 Quiaoit (2005).

186 All shells were sectioned along the axis of maximum growth after removing epibionts using a
187 metal brush (see **Fig. 1G-I**). Original microstructure and preservation of the original aragonite
188 mineralogy of all specimens was confirmed using Scanning Electron Microscopy and X-ray
189 Diffraction Spectroscopy following Gannon et al. (2017) and Kontoyannis and Vagenas (2000)
190 (see details in Killam et al., 2020). Shell segments were partially embedded in Araldite 2020 epoxy
191 resin (Huntsman Corp., Woodlands, TX, USA) before being sectioned in direction of maximum
192 growth using a slow-rotating saw equipped with a thin wafered saw blade (thickness < 1 mm).
193 Parallel cross sections produced 5-10 mm thick sections that were polished using progressively
194 finer SiC polishing disks.

195

196 2.3 Microscopy and photography

197 Polished surfaces of all 11 cross sections (5 *Pecten*, 6 *Tridacna*) were imaged using an Epson®
198 1850 flatbed scanner (Seiko Epson Corp., Nagano, Japan) at a pixel resolution of 6400 dpi (±4
199 µm pixel size) as well as by stitching micrographs made using a KEYENCE VHX-5000 digital
200 microscope using x250 magnification together into composite images (see **S1**). Cross sections

were imaged both before and after trace element analyses to allow the trace element profiles to be referenced relative to the cross sections.

2.4 LA-ICP-MS analyses

Elemental ratios were based on measuring ratios of the isotopes ^{25}Mg, ^{87}Sr, ^{55}Mn and ^{137}Ba to ^{43}Ca along profiles through all shell cross sections using Laser Ablation – Inductively Coupled Plasma – Mass Spectrometry (LA-ICP-MS). Measurements were carried out on a laser ablation system (ESI NWR193UC; Elemental Scientific, Omaha, NE, USA) coupled to a quadrupole ICP-MS (iCap-Q, Thermo Fisher Scientific, Waltham, MA, USA) at the Royal Netherlands Institute for Sea Research (NIOZ). Operation parameters are provided in **S11**.

Scan lines were programmed on the polished shell cross-sections in direction of growth as close as possible to the outer edge of the shell, with the rectangular LA-ICP-MS spot oriented parallel to the growth lines (with a width of 20 µm in scanning direction, see **Fig. 1J**; **S11**). For the pectinids, care was taken to target the outer portion of the outer shell layer (oOSL) and avoid sampling of the inner portion of the outer shell layer (iOSL) or inner shell layer (ISL), which was demonstrated to have a different chemical composition (see Freitas et al., 2009). For the tridacnids, profiles were placed within the OSL close to (within 100 µm of) the outer edge of the shell in a first analytical session. However, since spikes of high Mg/Ca and Mn/Ca ratios were observed in these results, parallel transects placed approximately 100 µm further towards the inside of the shell were measured through all tridacnid shells to verify whether these spikes in Mg and Mn were reproducible further inward (see **S2**). The combination of laser scan speed (4 µm s^{-1}) and ICP-MS run cycle time (“sweep time”; 109 ms) yielded a mean spatial sampling resolution of 0.44 µm, determined as the arithmetic mean without considering the shape of the laser spot. However, note that the width of the LA-ICP-MS spot size in scanning direction (20 µm) caused

smoothing of the LA-ICP-MS signal, reducing the effective spatial sampling resolution. As a result, each 0.44 µm wide segment of the shells in growth direction is sampled 45 times while the spot moves across the shell. We tested the effect of this smoothing on a virtual record with characteristics similar to the Sr/Ca record obtained by Sano et al. (2012) (see **section 3.3** and **S13**). All scan lines in pectinids and tridacnids were repeated a second time at the exact same location using a faster scan rate of 10 µm s^{-1} to assess repeatability of the elemental signals (see **S2**).

Data reduction was performed using an adapted version of the data reduction software SILLS (Signal Integration for Laboratory Laser Systems; Guillong et al., 2008) in Matlab. Raw LA-ICP-MS data were calibrated using NIST610 (National Institute of Standards and Technologies, Gaithersburg, MD, USA) using the reference values reported in the GeoReM database (Jochum et al., 2005, 2011). Quality control reference materials BAS CRM 393 (Bureau of Analyzed Samples, Middlesbrough, UK), RS3 and one matrix-matched carbonate standard (MACS-3; United States Geological Survey, Reston, VA, USA; Wilson et al., 2008) were used to monitor the quality of the measurement. Details on the accuracy of the LA-ICP-MS trace element results relative to preferred values for the check standards are provided in **S12**.

To increase the stability of the ICP-MS signal and to correct for drift, ^{43}Ca was used as internal standard. Calcium concentrations were assumed to be constant (38 wt%) throughout the LA-ICP-MS profiles within the same shell layer. External drift-correction using repeated measurements on the JCp1 standard was applied. The element/Ca drift was less than 5 % during the analytical sequence. Drift during a single transect was found to be negligible.

2.5 Age models

Trace element profiles in *P. maximus* shells were internally dated using daily striae visible on the outer shell surface (**Fig. 1D**). Daily increment widths (perpendicular distances between successive striae) were counted and measured multiple times, both on the outside of the shell using the focus-stacked images (see **section 2.3**) and by counting and measuring the distance between growth layers in cross sections through the "valleys" of the shells (**PM2_2** and **PM3_2**; see **S3**) by different persons. Positions of daily striae on the outside of the shells were plotted relative to distance along the LA-ICP-MS scan line using manual alignment of striae and the LA-ICP-MS path on microscope composites of cross sections through the shells, taking into account the curvature of growth lines with distance away from the outer shell surface (see **S3**). The timing of shell formation was determined by backdating the daily striae from the ventral margin (last visible stria mineralized on the date of shell collection, i.e., November 15, 2019), and by linearly interpolating the timing of measurements located between daily growth lines based on their distance from daily striae positions (**S5**).

Trace element profiles from *Tridacna* shells were also dated using layer counting. Polished cross sections through all tridacnids were imaged using UV luminescence (see **Fig. 1J** and **S4**) and stained with Mutvei solution (Schöne et al., 2005c; Killam et al., 2021) to facilitate this counting. However, despite staining and luminescence techniques, the expression of daily and semi-diurnal (half-daily, or 12h rhythmic) growth markings were insufficiently clear to count individual growth lines along the full (multi-year) growth period recorded in all the shells. Therefore, we opted for a hybrid method in which we measured the width of daily and semi-diurnal increments in parts of cross sections of each shell where they were well developed and used these measurements in combination with the annual growth breaks (which are easily recognized on the shell) to create age models for all specimens. The distinction between diurnal (24 h) and tidal (~12 h) pacing of growth increments was made based on the width of small-scale increments relative to the width of annual increments in the shell. A von Bertalanffy growth model (Von Bertalanffy, 1957) was

constructed for each specimen based on the annual growth (∆L) inferred from (semi-)diurnal growth line counting and the maximum shell height (L_{inf}) known for these species in the Red Sea from the literature (Roa-Quiaoit, 2005; Mohammed et al., 2019):

$$L_t = L_{inf} * \left(1 - e^{-kt}\right), with\ k = -ln\left(\frac{\Delta L}{L_{inf}}\right)$$

In this formula, L_t is the shell height at time t and k is the growth constant (Brody growth coefficient; Munro, 1982). Since cross sections through the tridacnids were made through the shell hinge (in direction of the shell height) and literature values for L_{inf} are reported with reference to shell length (measured parallel to the shell hinge), allometric data on *T. maxima*, *T. squamosa* and *T. squamosina* from the literature was used to convert L_{inf} values (which are commonly reported as shell length) to shell height and make them relevant for the direction in which the trace element profiles were measured on the cross sections (Roa-Quiaoit, 2005; Richter et al., 2008; Mohammed et al., 2019). Uncertainties on the annual growth increment widths (∆L) were calculated from the standard error of the mean width of daily and semi-diurnal growth increments on which ∆L is based, and uncertainties on the values for L_{inf} were taken from variability in the values in the literature. Both sources of uncertainty were propagated through the growth model using the variance formula (Ku, 1966) to obtain error envelopes on age-distance relationships (growth curves) of tridacnids (see **S5**). All data processing steps described in this manuscript are carried out using the open-source computational software package R (R Core Team, 2013), and scripts detailing these calculations are provided in **S6** and deposited on the open-access software repository GitHub (https://zenodo.org/record/6603175)

2.6 Spectral analysis

Spectral analysis on the LA-ICP-MS data was used to isolate trace element variability at the sub-annual scale. All trace element profiles were first detrended using a LOESS filter with a span of 0.2 times the length of the record to remove longer term (i.e., seasonal to multi-annual) trends. The detrended series were linearly resampled in the time domain before applying the Multi-Taper Method (MTM; Thomson, 1982) to extract dominant frequencies from the data. Spectral analysis was carried out using the "astrochron" package (Meyers, 2014) in R (R Core Team, 2013; see script in **S6**). The significance of relevant periodicities was tested using a combination of "red noise" estimation and a harmonic F-test (see Meyers, 2012). To visualize the evolution of periodic behavior across the shells, wavelet analysis was applied on all trace element profiles using the "dplR" package in R (see **S6**).

2.7 Extracting high-resolution variability

After detrending and spectral analysis, all trace element profiles were smoothed using a Savitzky-Golay filter with a width of 21 datapoints (8.4 µm; equivalent to a timespan of ~1-5 h; **S6**) to remove high-frequency measurement noise within our LA-ICP-MS spot size. The Savitzky-Golay filter was used because it preserves the tendency of the trace element profile and therefore retains a larger fraction of the amplitude of periodicity close to the width of the filter compared to simpler smoothing techniques (e.g. moving average; Savitzky and Golay, 1964). The 21-point window size was chosen to smooth out the maximum amount of instrumental noise without losing periodicity larger than half the width of the laser spot (0.22 µm; equivalent to 23 datapoints). Statistically significant (see **section 2.6**) variability in daily (~22-36 h; centered on the 24 h diurnal cycle) and semi-diurnal (~8-14 h; centered on the 12.4 h tidal cycle) frequency bands was extracted from the trace element records using a combination of bandpass filtering (using the "bandpass" function in the "astrochron" R package) and stacking (see **S6**). Trace element data was stacked along bandpass filters using the following procedure: Maxima and minima in the

bandpass filter were used as tie points to reference each datapoint of the smoothed dataset relative to its position within the cycle on a scale from 0 to 1. These relative positions were then used to divide the data into 10 bins (bin 1 contains positions 0 – 0.1, bin 2 contains data from positions 0.1 – 0.2, etc.), providing stacked data a resolution of 0.1 times the length of the cycle under investigation. The full breakdown of variability within and between bins created in the stacking routine is provided in **S7**. Different sources of variance in the trace element records were isolated by sequentially determining the variance left in the trace element records after each of the data treatment steps explained above (see example in **S7**). This procedure allowed us to quantify the amount of variance in each trace element profile explained by either diurnal or semi-diurnal variability.

3. Results

3.1 Trace element data

LA-ICP-MS line scans yielded profiles of Sr/Ca, Mg/Ca, Mn/Ca and Ba/Ca in growth direction on 11 cross-sections through shells of *P. maximus*, *T. maxima*, *T. squamosa* and *T. squamosina* (**Fig. 2**; see **S0** for raw data of all scans). Sub-millimeter scale patterns in Sr/Ca, Mg/Ca, Mn/Ca, and Ba/Ca are highly reproducible between consecutive line scans on the same LA-ICP-MS transect: R^2 values typically exceed 0.8, and mean element ratio differences between time equivalent samples in different line scans are typically <0.05 mmol mol^{-1} for Mg/Ca (<5 % relative to mean value), <0.02 mmol mol^{-1} for Sr/Ca (<2 % relative to mean value), <0.5 µmol mol^{-1} for Mn/Ca (<10 % relative to mean value) and <0.2 µmol mol^{-1} for Ba/Ca (<8 % relative to mean value; see **S2**). Remeasured transects further away from the outer shell surface in tridacnids (see **section 2.4**) differ more from the original transects than those measured on the exact same locality in the shell: R^2 values between parallel lines in different localities are 0.3 – 0.5 for Mg/Ca and Sr/Ca and <0.3 for Mn/Ca and Ba/Ca, reflecting intra-shell variability in trace element composition in the tridacnids (**S2**). Overall, sub-millimeter scale patterns in trace element composition are reproduced in parallel line scans. Finally, “rib” and “valley” segments through the same specimen of *P. maximus* show similar patterns in trace elements, but element-to-calcium ratios (especially Ba/Ca and Mn/Ca) can be quite different, highlighting heterogeneity within the shells of *P. maximus* (**Fig. 2**).

Trace element profiles in pectinids, reflecting only one growing season, show Sr/Ca and Mg/Ca maxima in the middle of the profile, while Mn/Ca and Ba/Ca are more variable, showing multiple peaks in the same growth year. Peaks in Mn/Ca and Ba/Ca are synchronous between profiles through the same specimen, but not between specimens. Tridacnid Mg/Ca, and Sr/Ca ratios show one or two distinct cycles per growth year. Mn/Ca and Ba/Ca ratios in tridacnids show more regular annual or biannual variability than pectinids (most notably specimen **SQSA1**). It must be

noted, however, that *P. maximus* shells only recorded one growth season, limiting the interpretation of seasonal growth patterns.

Plots of trace element variability zoomed in on smaller sections of the record reveal dominant high-frequency variability superimposed on seasonal-scale patterns (**Fig. 3**). Both tridacnid and pectinid LA-ICP-MS records show distinct high-frequency cyclicity in all studied trace element-to-Ca ratios with amplitudes on nearly the same order of magnitude as the longer-term variability described by the records on a seasonal to multi-annual scale (**Fig. 2**).

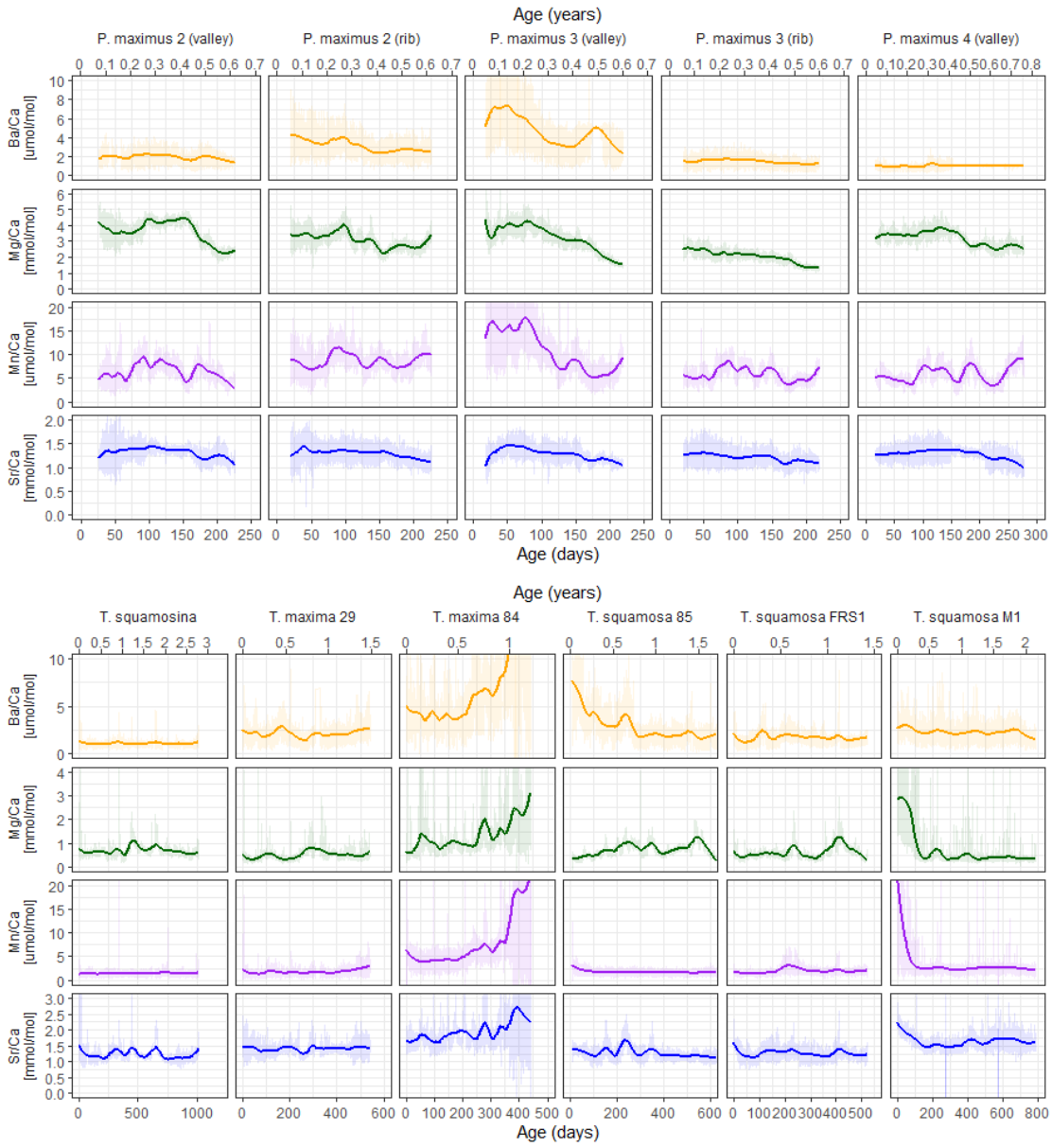

362

363 Figure **2**: Overview of LA-ICP-MS results of Sr/Ca (blue), Mg/Ca (green), Mn/Ca (purple) and
364 Ba/Ca (orange) in pectinid (upper panel) and tridacnid (lower panel**)** specimens. Vertical axes are
365 equal for plots positioned next to each other (but different for the two groups of tridacnid and
366 pectinid plots). Shaded lines show raw LA-ICP-MS data while solid lines indicate 0.2 span LOESS
367 fits through the data highlighting monthly-scale variability. A direct comparison of trace elemental
368 ratios between specimens is provided in **S8**.

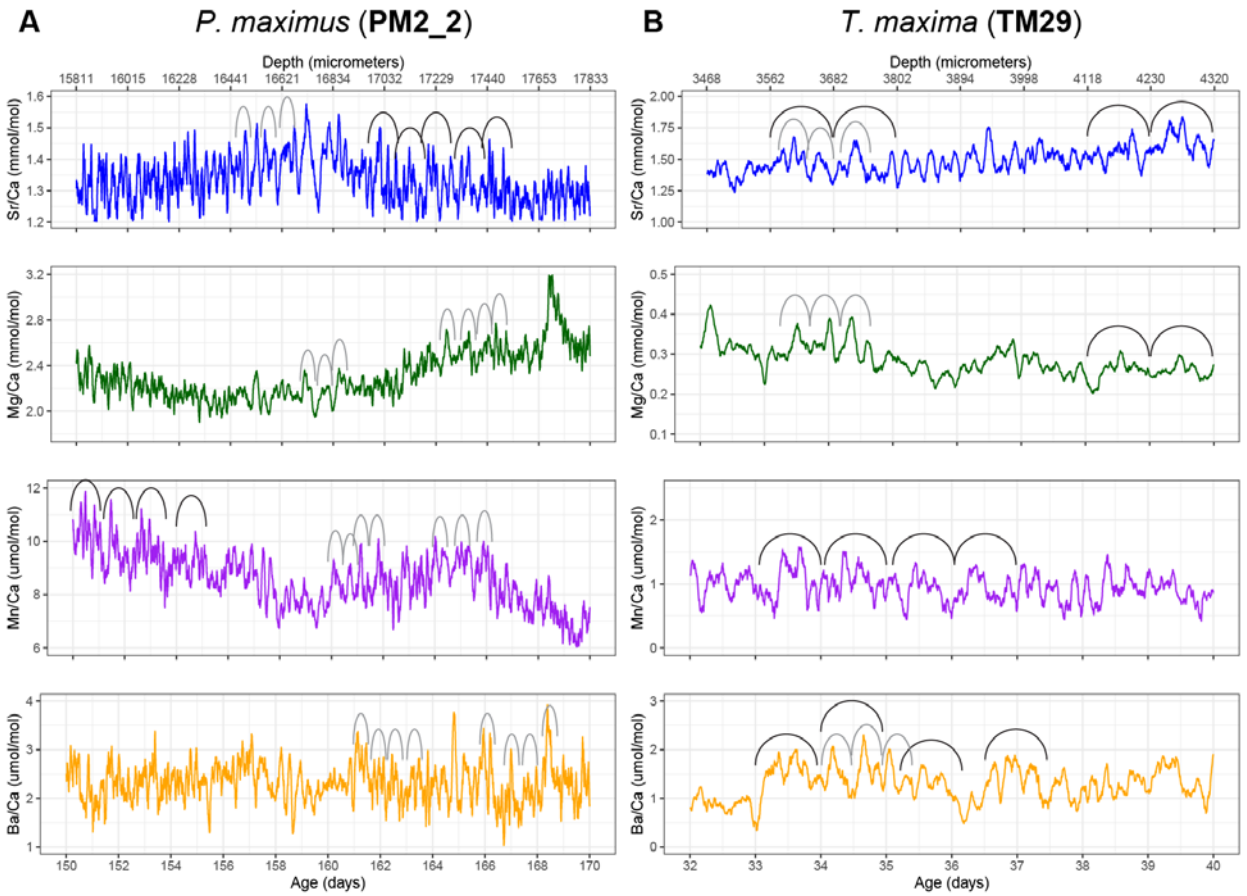

Figure 3: Plots showing samples of semi-diurnal and daily variability in Savitzky-Golay filtered trace element ratios in selected intervals through *P. maximus* specimen **PM2_2** (**A**; 51-point filter) and *T. maxima* specimen **TM29** (**B**; 21-point filter). Filters isolate hour to daily scale variability while filtering out the higher-order measurement noise. Arches indicate examples of the expression of daily (black) and semi-diurnal (grey) cycles in the records.

375

376 3.2 Age models

377 Growth line counting in the *P. maximus* shells was repeated multiple times on both the outer shell
378 surface and in cross sections through the shell by different persons (**Table 1**; **S3**). The variability
379 in counting results shows that the growth lines were not always equally easy to distinguish. In
380 **PM2** and **PM3**, the most likely number of increments (228 and 220 respectively) was confirmed
381 in both cross sections and on the outside of the shell. In **PM4**, counting in the cross section (278
382 increments) was chosen over the slightly lower count on the outside of the shell (272-273
383 increments) since the LA-ICP-MS profile was measured on the same cross section and could be
384 directly linked to the counted increments. Note that, while the consistency in daily counts between
385 specimens from the same year and environment is encouraging, inter-specimen variability in the
386 onset of spring growth or the onset of the winter stop (potentially prior to the collection date of
387 November 15th, 2019) places some uncertainty on the absolute date assigned to *P. maximus* shell
388 sections (Chauvaud et al., 2005). The age-distance relationships (growth curves) resulting from
389 the sclerochronology are shown in **S5**.

390

Table 1: Growth increments counting in *P. maximus* Values separated by comma's refer to different counts at the same location of the same specimen. Values in bold indicate counts closely corresponding between cross section and outer shell surface.

Specimen	Increments counted on outer surface	Increments counted in cross sections	Mean daily increment width [µm ± 1σ]
PM2	226, **228**, 234, 241	227, **228**, 233	249 ± 19
PM3	**220**, 226, 243	213, **220**, **220**	249 ± 22
PM4	272, 273	**278**	247 ± 4

Layer counting in tridacnid shells yielded estimates of semi-diurnal, daily and annual growth (**Table 2**; **S4**). Annual growth rates calculated from layer counting are highly consistent between specimens from the same species from the same environment (within 1 mm yr^{-1}; **Table 2**), lending confidence to the growth line counting results. The von Bertalanffy growth models based on these growth line counts are plotted in **S5**. Statistics of the parameters (L_{inf} and k) of these growth models and their uncertainty are provided in **S4**.

Table 2: Growth line counting in *Tridacna* shells. Column 3 shows the total number of increments counted in the specimen, column 4 shows their median width and column 6 shows the width of an annual increment in the specimen. Note that increments could not be counted over the entire growth period of the shells, so the numbers in column 3 represent representative numbers of increments counted in those parts of the shells where they were distinct enough for counting (see **section 2.5**). Increment timing (semi-diurnal vs diurnal) was established based on the relative difference between increment width and the distance between annual growth breaks measured on the outside of the shells (see **S4** for details).

Specimen	**Species**	**# counted increments**	**Median increment width [µm]**	**Mean increment width**	**Annual growth [mm]**	**Increment timing**
TM29	*T. maxima*	274	26.5	28.7	27.9	Semi-diurnal
TM84	*T. maxima*	109	39.1	40.2	26.6	Diurnal
TS85	*T. squamosa*	310	40.3	40.5	20.2	Diurnal
TSFRS1	*T. squamosa*	225	23.3	24.5	20.1	Semi-diurnal
TSM1	*T. squamosa*	180	33.3	34.4	20.6	Diurnal
SQSA1	*T. squamosina*	153	22.3	22.3	14.9	Diurnal

3.3 Growth rates and temporal sampling resolution

Growth rates are highly similar between specimens of the same species (**Table 1 and Table 2**; **S3-5**), with *P. maximus* achieving the highest growth rates (~ 220 growth days * ~ 250 µm/d ≈ 55 mm/yr; **Table 1**), followed by *T. maxima* (~27 mm/yr; **Table 2**), *T. squamosa* (~20 mm/yr; **Table 2**) and *T. squamosina* (15 mm/yr; **Table 2**). Dividing the width of the daily increments (e.g., 250 µm for *P. maximus*) by spatial LA-ICP-MS sampling resolution of 0.44 µm (see **section 2.4**), these growth rates would seem to translate to a temporal resolution of 0.04 h, 0.24 h, 0.44 h and 0.27 h for *P. maximus*, *T. maxima*, *T. squamosa* and *T. squamosina*, respectively. However, our LA-ICP-MS spot size (20 µm in sampling direction) causes significant smoothing, reducing the frequency that can be resolved. Nevertheless, our test applying the LA-ICP-MS settings on a virtual Sr/Ca dataset with the characteristics of the diurnal record by Sano et al. (2012) and growth rates equivalent to our specimens (see **S13**) reveals that our analytical methodology can easily resolve daily variability even in our slowest-growing specimen (*T. squamosina* **SQSA1**), conserving at least 75 % of the signal amplitude. The LA-ICP-MS profiles record trace element variability during growth periods ranging between 220 days (for **PM3**) and 1041 days (for **SQSA1**).

3.4 Spectral analysis

Normalized power spectra and significance level of daily and tidal periodicities in pectinid and tridacnid records are shown in **Figure 4** and **Figure 5**, respectively. Full spectral analysis results for all trace element records in all specimens are provided in **S9**. All *P. maximus* power spectra (**Fig. 4**) reveal semi-diurnal (12 h) periodicity in Sr/Ca and Ba/Ca with > 86 % statistical significance. Only sections through the ribs of the shells (**PM2_1** and **PM3_1**) show semi-diurnal periodicity in Mg/Ca and Mn/Ca (> 90 % significance). Daily periodicity is present in some, but not all, pectinid profiles. Most pectinid trace element records also contain multi-day periodicities,

including strong 7-day periodicities and weaker cyclicity associated with 14-day and 28-day cycles. The latter is partly suppressed by the 0.2 span LOESS filter (equivalent to a 44–56-day period depending on the length of the record) applied on the records to remove the seasonal trend from the records. However, these lower frequency cycles are clearly visible in the wavelets (see **S9**).

Tridacnid trace element profiles show more consistent daily periodicity than pectinid records (**Fig. 5**). Especially Sr/Ca and Ba/Ca records through nearly all tridacnid specimens exhibit strong (> 90 % confidence level) power in the daily period, while daily cyclicity is weaker in Mn/Ca and Mg/Ca records. Sr/Ca records in the tridacnids also contain a significant (> 96 %) semi-diurnal component, whose tidal origin seems clear in most specimens by peaks in power in the longer (7 d, 14 d and 28 d) tidal components.

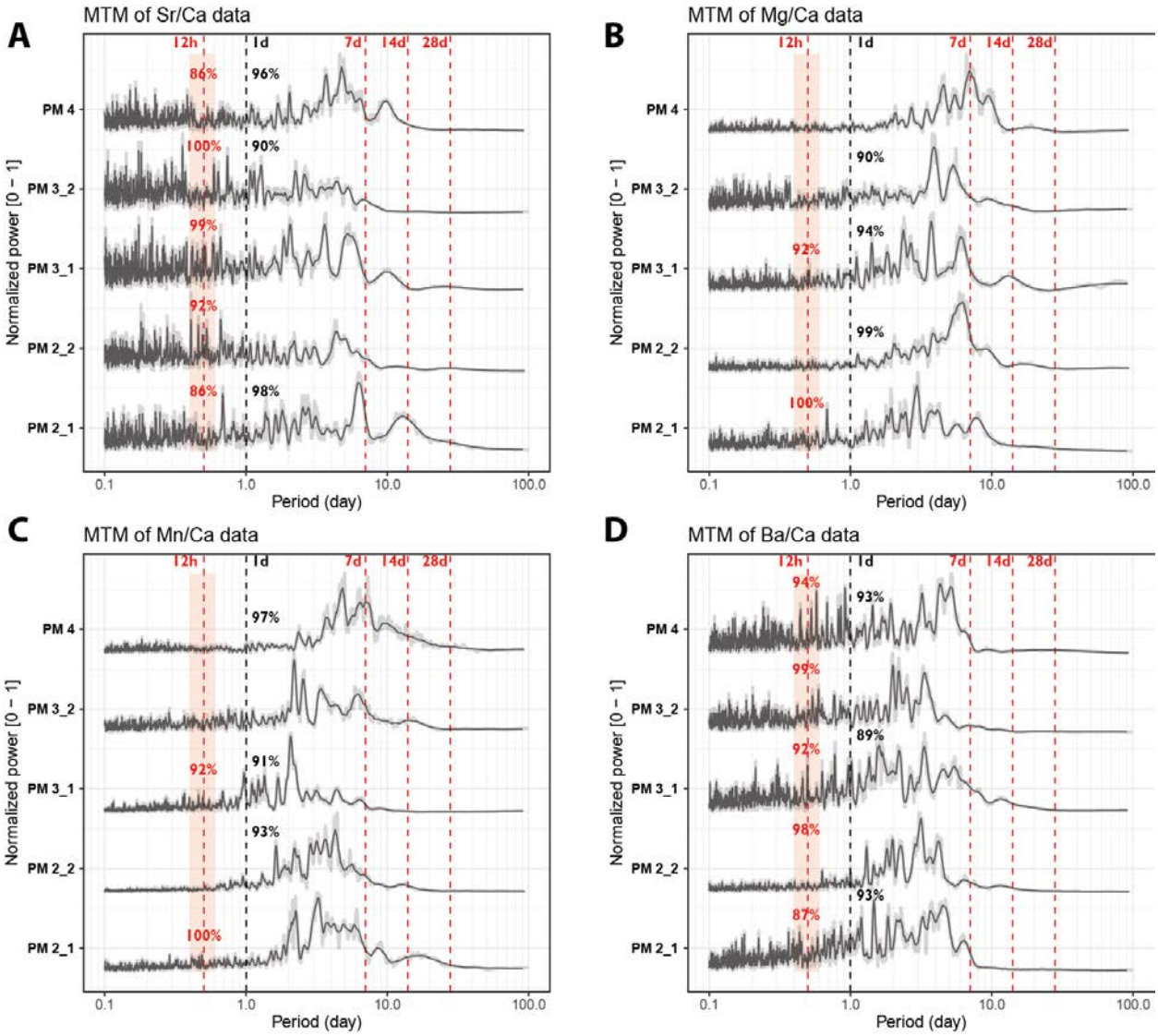

Figure 4: Multi-taper method spectrograms of Sr/Ca (**A**), Mg/Ca (**B**), Mn/Ca (**C**) and Ba/Ca (**D**) records through the five pectinid cross sections after detrending (see **section 2.6**). All spectra are normalized by dividing by the highest power peak and plotted on the same horizontal axis. Grey shaded lines show raw data while solid black lines plot 21-point moving average smoothed curves. Red vertical dashed lines highlight the expected periods of tidal variability while black vertical dashed lines indicate 1-day periodicities. Significance levels of peaks on these periods (see **section 2.6** and Meyers, 2012) are rounded to the nearest whole percentage point.

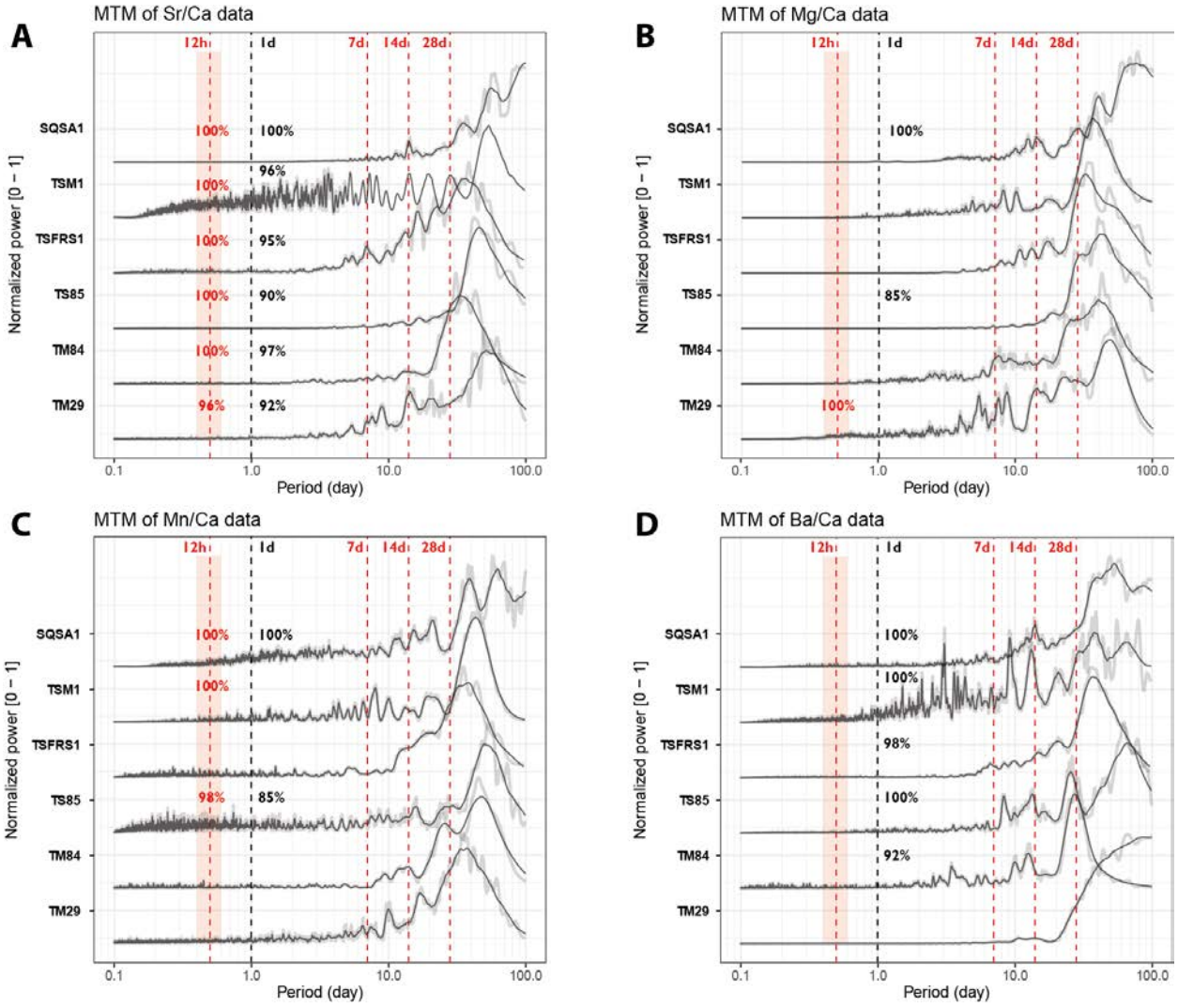

456

457 **Figure 5**: Multi-taper method spectrograms of Sr/Ca (**A**), Mg/Ca (**B**), Mn/Ca (**C**) and Ba/Ca (**D**)
458 records through the six tridacnid cross sections after detrending (see **section 2.6**). All spectra are
459 normalized by dividing by the highest power peak and plotted on the same horizontal axis. Grey
460 shaded lines show raw data while solid black lines plot 21-point moving average smoothed
461 curves. Red vertical dashed lines highlight the expected periods of tidal variability while black
462 vertical dashed lines indicate 1-day periodicities. Significance levels of peaks on these periods
463 (see **section 2.6** and Meyers, 2012) are rounded to the nearest whole percentage point.

464

3.5 Variance decomposition

Variability at the daily (24 h) and semi-diurnal (12 h) scale in all trace element records through all specimens was extracted using bandpass filtering (**section 2.7;** see **S9** and **S10**). The median amplitude of variability within these stacks was plotted against the median period of the variability per element and per specimen to highlight dominant periodicities in the trace element data (**Figure 6**). As noted in the spectral analysis results (**section 3.4**), trace element composition in tridacnid shells is more strongly controlled by daily variability than in pectinid shells (**Fig. 6**; **S10**). The difference is especially noticeable in Sr/Ca and Ba/Ca ratios, which show a clear divide between daily periodicity in tridacnid shells and tidal periodicity in pectinids (see **Fig. 6**). The differences in Mg/Ca and Mn/Ca ratios are less obvious.

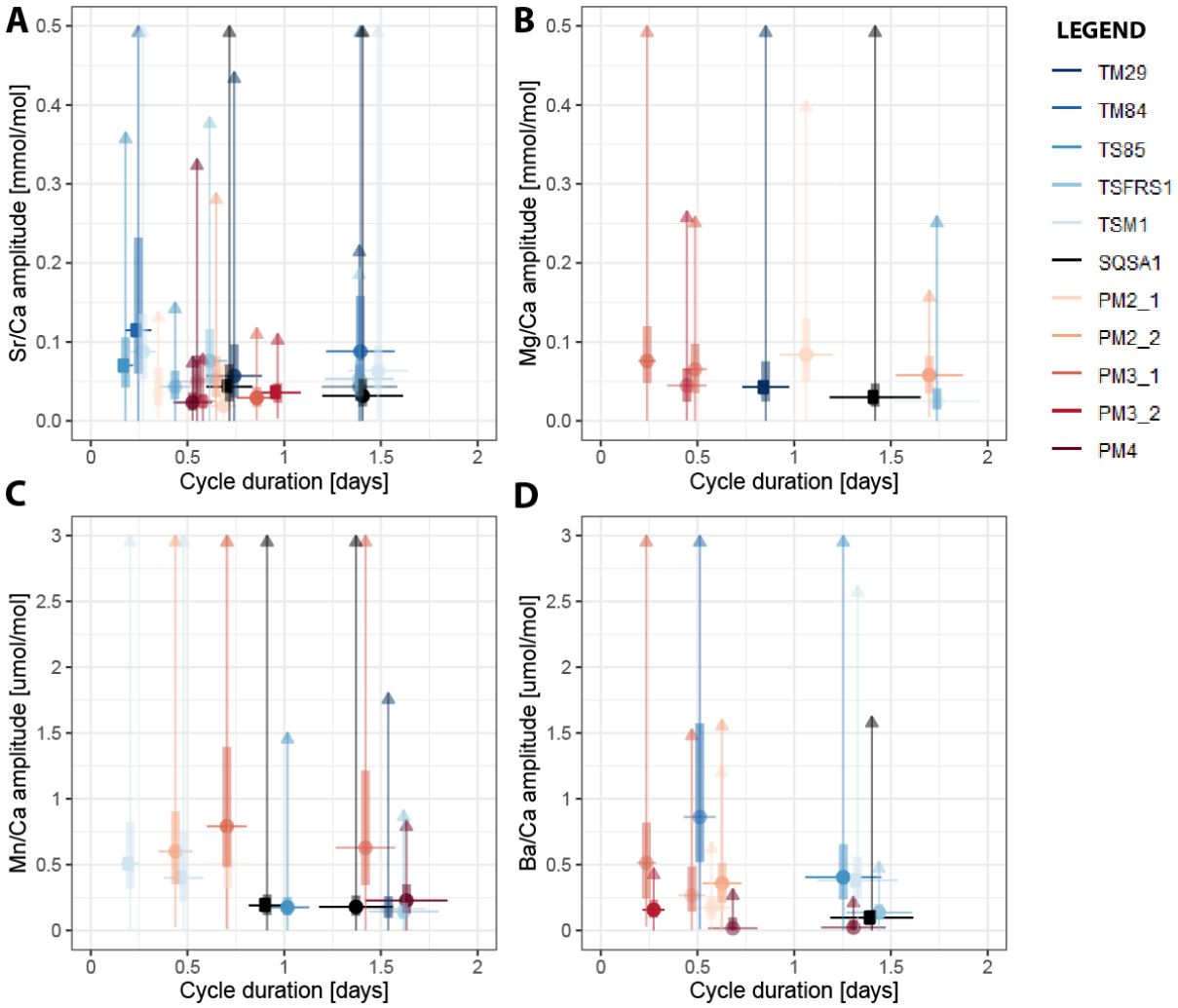

476

477 **Figure 6:** Cross plot showing the amplitude of variability of dominant spectral periods in Sr/Ca
478 (**A**), Mg/Ca (**B**), Mn/Ca (**C**) and Ba/Ca (**D**) against the period (duration) of the cycle. Round
479 symbols indicate the median amplitude of the cycle, while vertical bars and lines show interquartile
480 differences and ranges in the amplitude over the record. Horizontal bars indicate the width of the
481 bandpass filter used to extract periodic variability. Colors highlight different specimens (see
482 legend).

483

An example of the distribution of normalized variability within the trace element records after each data processing step is shown in **S7**. This example shows that a large fraction of the variance in the records (73 % in this record after trimming outliers) is explained by low-frequency (seasonal scale) variability (**S7**). Of the remaining smoothed and detrended dataset, at most 20 % of the variance is explained by daily and tidal (semi-diurnal) periodicity (see **Figure 7** and **Table 3**). A full decomposition of variance in all trace element records through all specimens is provided in **S7**. **Figure 6** and **Figure 7A** show that, overall, the variance explained by daily periodicity is higher in tridacnids than in pectinids (Wilcoxon signed rank test; $W = 44$; $p = 0.009$). The difference between species is smaller for tidal variability (**Fig. 7B**). There is no clear difference in relative dominance of semi-diurnal variability between trace element records, but daily variability is more strongly expressed in Ba/Ca and Mn/Ca records, especially in tridacnid shells. Finally, *T. squamosa* specimen **TSM1**, which grew under a sunshade, does not exhibit significantly lower daily periodicity compared to the other tridacnid specimens.

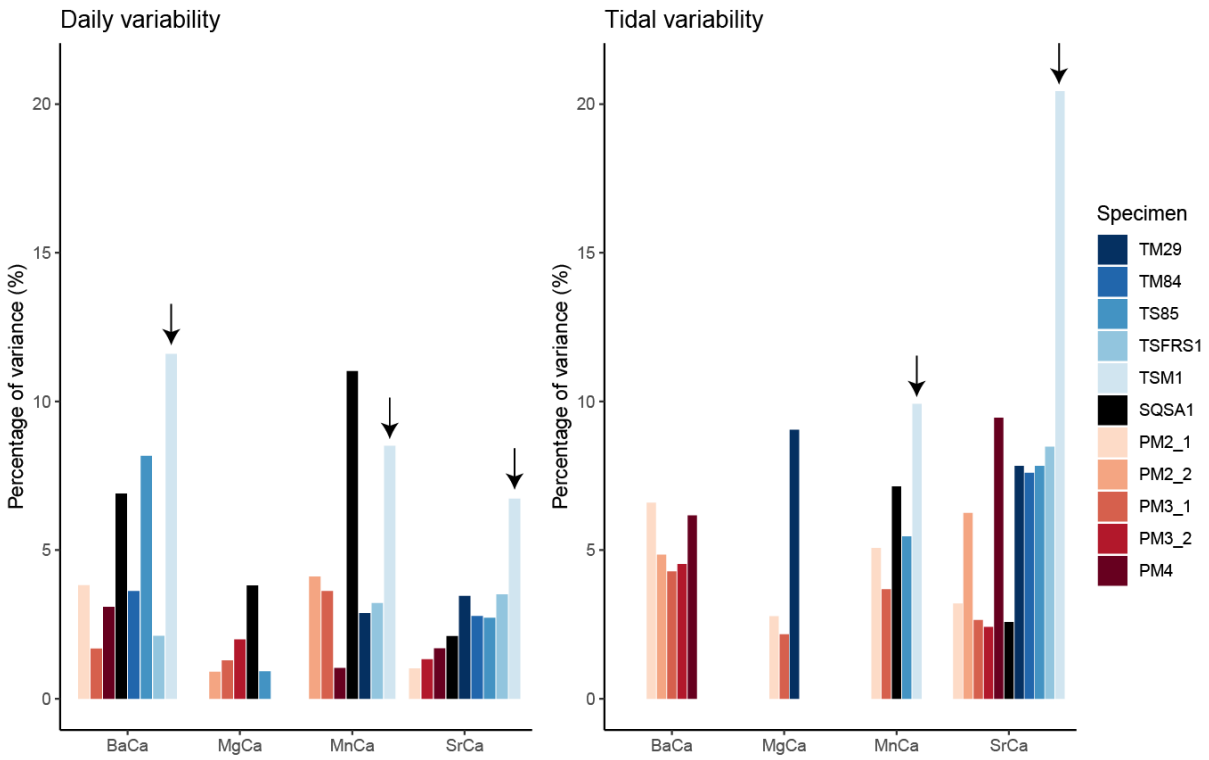

498

499 **Figure 7:** Summary of relative variance (in %) of significant daily (left) and tidal (right) variability

500 extracted from trace element records. Colors highlight different specimens (see legend). Note that

501 the *T. squamosa* specimen **TSM1** which grew under a sunshade is highlighted with a black arrow.

502

503 **Table 3**: Overview of the relative (in %) variance associated with daily and tidal variability in all
504 trace element records through all specimens. Empty cells represent records for which no
505 significant tidal or daily periodicity was found (see **Fig. 4-5**).

	Daily variance [% relative to detrended record]				**Tidal variance [% relative to detrended record]**			
	Ba/Ca	**Mg/Ca**	**Mn/Ca**	**Sr/Ca**	**Ba/Ca**	**Mg/Ca**	**Mn/Ca**	**Sr/Ca**
PM2_1	3.8 %			1.0 %	6.6 %	2.8 %	5.1 %	3.2 %
PM2_2		0.9 %	4.1 %		4.9 %			6.3 %
PM3_1	1.7 %	1.3 %	3.6 %		4.3 %	2.2 %	3.7 %	2.7 %
PM3_2		2.0 %		1.3 %	4.5 %			2.4 %
PM4	3.1 %		1.0 %	1.7 %	6.2 %			9.5 %
TM29			2.9 %	3.5 %		9.0 %		7.8 %
TM84	3.6 %			2.8 %				7.6 %
TS85	8.1 %	0.9 %		2.7 %			5.5 %	7.8 %
TSFRS1	2.1 %		3.2 %	3.5 %				8.5 %
TSM1	12 %		8.5 %	6.7 %			10 %	20 %
SQSA1	6.9 %	3.8 %	11 %	2.1 %			7.1 %	2.6 %

506

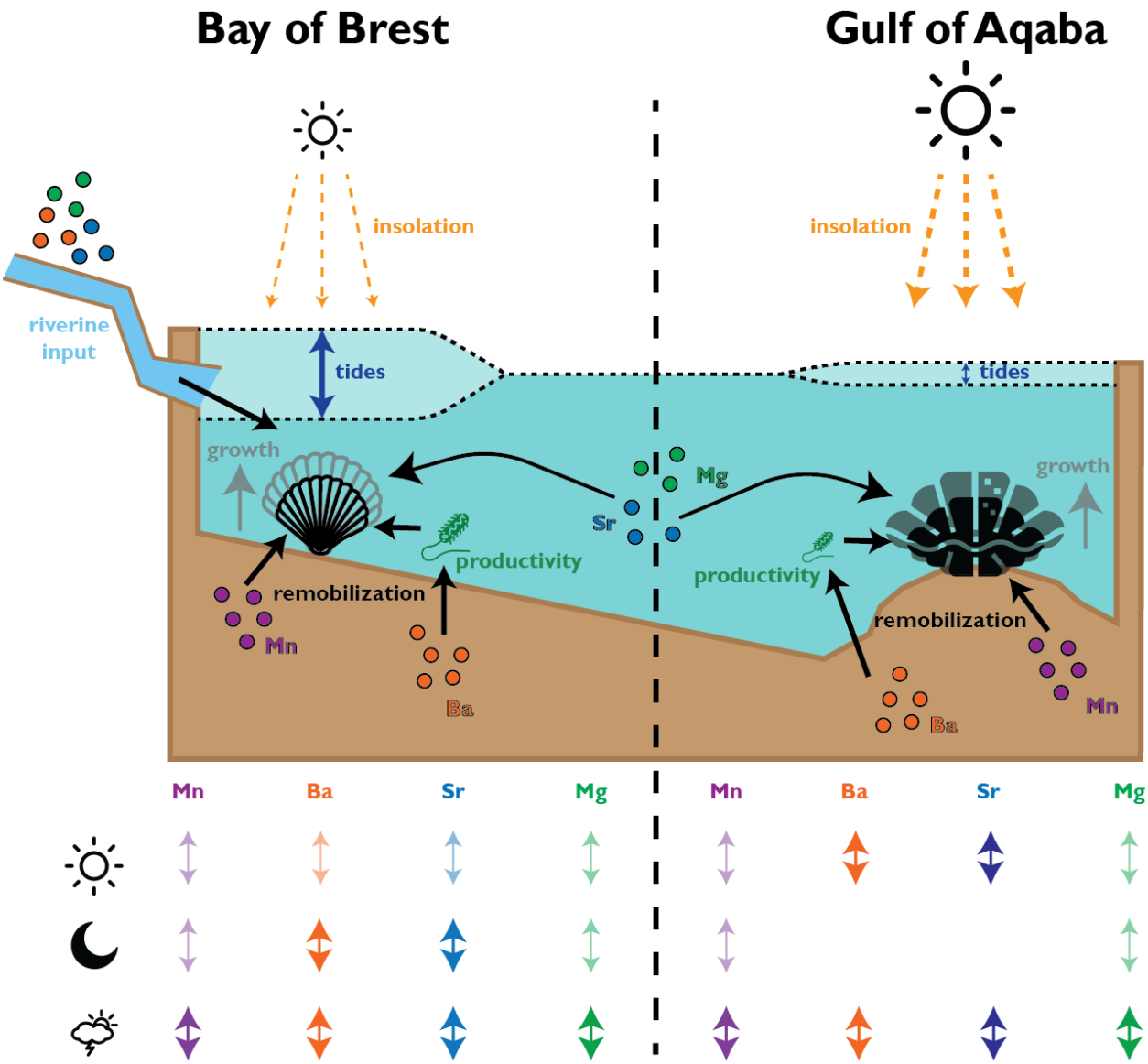

507

508 **Figure 8**: Schematic overview of environmental parameters interpreted to affect shell growth and
509 composition of pectinids in the Bay of Brest and tridacnids in the Gulf of Aqaba. The table at the
510 bottom provides a schematic qualitative overview of the amount of variance in the trace element
511 records of the taxa is explained by daily (sun symbol), tidal (moon symbol) or aperiodic (cloud
512 symbol) variability in the environment.

513

4. Discussion

4.1 Compositional differences between pectinids and tridacnids

Pectinid and tridacnid shells are characterized by similar mean Sr/Ca and Ba/Ca ratios (Sr/Ca of 1.3 ± 0.3 and 1.5 ± 0.6 mmol mol^{-1} respectively; Ba/Ca of 2.8 ± 2.5 and 3.0 ± 5.1 µmol mol^{-1} respectively; uncertainty is calculated as 1 σ). Mean Mg/Ca and Mn/Ca ratios are higher in *P. maximus* than in *Tridacna* species (Mg/Ca = 3.1 ± 0.9 and 0.7 ± 0.9 mmol mol^{-1}; Mn/Ca = 7.8 ± 4.7 and 2.7 ± 7.8 µmol mol^{-1}; 1 σ; **Figure 2**; **S4**). The incorporation of higher concentrations of the elements Mg and Mn, which have a smaller ionic radius than Sr and Ba, in calcitic pectinid shells compared to aragonitic tridacnid shells makes sense given the higher partition coefficient of these elements in calcite than in aragonite (Day and Henderson, 2013; Wassenburg et al., 2016).

Differences between tridacnid specimens generally exceed the differences between tridacnids and pectinids (1σ of Ba/Ca among all tridacnid specimens = 2.1 µmol mol^{-1}), suggesting large inter-species differences. However, individual records such as those in **TM84** and **PM3_1** show large variability (especially in Ba/Ca and Mn/Ca) compared to other specimens of the same species. Inter-specimen variability is higher in tridacnid shells than in pectinids (inter-specimen relative standard deviations as a fraction of mean ratio for Ba/Ca: 0.74 vs 0.64 µmol mol^{-1}, Mg/Ca: 0.37 vs 0.20 mmol mol^{-1}, Sr/Ca: 0.19 vs 0.03 mmol mol^{-1} and Mn/Ca: 0.78 vs 0.33 µmol mol^{-1} for tridacnids and pectinids, respectively). **Figure 2** shows that this variability between tridacnids is not readily explained by differences between species, but mostly reflects differences in the trends within the records, with some specimens (e.g., **TM84**, **TSM1** and **TS85**) showing trends in composition towards the end of the record (see also **S8**). It thus seems that inter-specimen differences, perhaps driven by growth stress, are dominant drivers of trace element variability in giant clams. This interpretation is corroborated by the observation that trace element compositions in tridacnid shells are significantly more skewed towards higher values than in pectinids (mean skewness per element and per specimen is 9.7 for tridacnids and 0.9 for

pectinids). This skewness reflects the high peaks in trace element composition observed in tridacnid profiles, especially near the ventral margin (e.g., specimens **TM84**, **TSM1** and **TS85**; see **section 2.4**; **Fig. 2**; **S8**), which hint towards growth disturbances at the individual level.

4.2 Trace element variability in *P. maximus*

4.2.1 Comparison with previous studies

Trace element concentrations in *P. maximus* analyzed in this study are in close agreement with concentrations found in wild (live collected) pectinid shells in the literature (Lorrain et al., 2005; Barats et al., 2008; Poitevin et al., 2020; Fröhlich et al., 2022). In these studies, Sr/Ca shows a strong link with calcification rate (as measured by the width of daily shell increments; Lorrain et al., 2005), although previous studies did not assess variability on the (sub-)daily scale. The long-term trends in our Sr/Ca records seem to confirm this correlation, with higher values being recorded in the middle of the growing season (day 50-150; **Fig. 2**) when growth rates are highest (see **S5**). Previous studies demonstrate that Mg/Ca ratios in pectinid shells are at most partially related to temperature and/or salinity (Lorrain et al., 2005; Poitevin et al., 2020). The fact that the studied *P. maximus* specimens, which all grew during the same year in the same environment, do not show a synchronous Mg/Ca pattern (**Fig. 2**) corroborates this previous work and argues against a straightforward temperature dependence for Mg/Ca in *P. maximus*. In addition, the lack of strict coherence between profiles of Mg/Ca (and other elements) in parallel transects through *P. maximus* shells (e.g., **PM2_1** and **PM2_2**; **Fig. 2**) hints at compositional heterogeneity within the shells, in agreement with findings by Lorrain et al. (2005). Low correlations between profiles through the same shell at the daily scale are also partly driven by small misalignments in the timing of shell formation between the transects at the sub-millimeter scale and variations in the height of trace element peaks, especially those of Mn/Ca and Ba/Ca, which are higher further towards the outside of the shell (**S2**).

There is evidence suggesting that Mg content varies in mollusk shells in function of the amount of organic matter in the biomineral (Dauphin et al., 2003; Richard, 2009; Tanaka et al., 2019). Contrarily, Mn is known to be taken up in thermodynamic equilibrium in the mineral fraction of bivalve shells (Onuma et al., 1979; Soldati et al., 2016), and Mn/Ca ratios in *P. maximus* have been shown to faithfully record fluctuations of dissolved Mn in the coastal environment driven by riverine input and redox conditions (Barats et al., 2008). Similarly, there is strong evidence that Ba/Ca ratios in *P. maximus* (and other mollusks) record changes in Ba available in the environment linked to primary productivity (e.g., Gillikin et al., 2008; Thébault et al., 2009; Fröhlich et al., 2022). Interestingly, our results (Fig. 2) show that background Ba/Ca values are not equal in the shells of *P. maximus* and tridacnid specimens grown in the same environment. This suggests that the findings by Gillikin et al. (2005) that background Ba/Ca concentrations are a function of environmental conditions and can be consistently subtracted from Ba/Ca records to separate peak from background values may not be generally valid. The suggested relationship between Ba/Ca and primary productivity would explain the skewed (skewness > 1; **S8**) character of the Ba/Ca records and the correlation between Ba/Ca and Mn/Ca in the studied *P. maximus* specimens, as reducing conditions following peaks in primary productivity favor the remobilization of Mn into the water column causing short-lived simultaneous increases in Ba/Ca and Mn/Ca in the shells (Dehairs et al., 1989; Barats et al., 2008, 2009).

4.2.2 Short-term changes in shell composition in *P. maximus*

In the context of the high-resolution trace element variability central to this study, it seems plausible that short-term changes in the environment of the Bay of Brest were drivers of Mn/Ca and Ba/Ca variability in *P. maximus* shells, while Mg/Ca and Sr/Ca composition is mostly driven by changes in calcification rate. This would suggest that the significant tidal (12 h) component in Ba/Ca and Mn/Ca records through *P. maximus* (**Fig. 4**) is driven directly by redox changes over the strong tidal cycle in the Bay of Brest (see Polsenaere et al., 2021) and resuspension of Ba

588 and Mn due to tidal currents (Hily et al., 1992), while tidal rhythms in Mg/Ca and Sr/Ca may be a
589 consequence of the scallop's calcification response to changes in its environment (e.g.,
590 temperature, salinity and light availability) through the large (up to 7 m range) tidal cycle (**Fig. 8**).
591 The latter corroborates with previous studies in other calcitic mollusk shells which demonstrated
592 that Mg incorporation on short timescales is driven by the metabolic response to subtle changes
593 in the environment (Lazareth et al., 2007). Finally, care must be taken to interpret trace element
594 variability in *P. maximus* shells, since large intra-shell gradients in Mg/Ca, Sr/Ca and Mn/Ca have
595 previously been observed in this species, making trace element composition highly dependent on
596 the location of measurements relative to the outer shell surface or positioning relative to striae on
597 the shell surface (Freitas et al., 2009). Even though the LA-ICP-MS line scans in this study
598 targeted exclusively the oOSL of *P. maximus* specimens, variability in elemental ratios resulting
599 from small changes in the distance of the line scan from the outer edge of the shell cannot be fully
600 excluded (Richard, 2009).

601

602 4.3 Trace element variability in tridacnids

603 4.3.1 Comparison with previous studies

604 Results for Sr/Ca, Mg/Ca and Ba/Ca in our tridacnid specimens broadly corroborate trace element
605 results in other tridacnid studies (e.g., Elliot et al., 2009; Sano et al., 2012; Yan et al., 2013; Warter
606 et al., 2018). While data on Mn/Ca in the OSL of tridacnids is scarce, the Mn/Ca ratios in tridacnids
607 in this study (mean Mn/Ca = 7.8 ± 4.7 µmol mol^{-1}) are similar to LA-ICP-MS Mn/Ca data available
608 in the literature (Warter et al., 2015, 4-10 µmol mol^{-1}), but significantly lower than Mn/Ca values
609 measured using total digestion Atomic Absorption Spectrometry (Madkour, 2005, ~30 µmol mol^{-1}).
610 The main difference between the techniques is that LA-ICP-MS (both in this study as in Warter
611 et al., 2015) sampled shell layers where growth lines were visible and did not include pre-

612 treatment, while the total digestion study (Madkour, 2005) removed organic matter by roasting
613 the shells at 200°C prior to bulk shell analysis. Given that Mn in bivalve shells is typically
614 associated with the mineral fraction of the shell (Soldati et al., 2016), the difference in results may
615 therefore hint at differences between shell layers within tridacnids, or differences in Mn
616 concentration between the organic and mineral fractions in the shells. Bivalve shells typically
617 contain between 1 % and 5 % organic matter (Marin and Luquet, 2004), with tridacnid shells being
618 notable for their low organic matter content (< 1 %; Taylor and Layman, 1972; Agbaje et al., 2017).
619 It thus seems unlikely that the differences in Mn/Ca ratio between bulk analyses (Madkour, 2005)
620 and *in situ* analysis (Warter et al., 2015; this study) could originate from variations within the
621 organic matrix, which only constitutes a small fraction of the shell. Therefore, we consider a
622 difference in Mn concentration between shell layers in tridacnids more likely. The lack of
623 consistent trace element offsets between the tridacnid species under study here (*T. maxima*, *T.*
624 *squamosa* and *T. squamosina*) confirms the chemical similarities between shells from various
625 tridacnid species found in previous studies (e.g., *T. gigas*; Elliot et al., 2009; Yan et al., 2013; *T.*
626 *crocea*; Warter et al., 2018; *T. derasa*; Sano et al., 2012).

627 4.3.2 Short-term variability in Sr/Ca paced to the day-night cycle

628 Sr/Ca in tridacnids is hypothesized to be strongly controlled by light intensity through a circadian
629 rhythm linked to the day-night cycle (Sano et al., 2012; Warter et al., 2018). This would explain
630 the strong daily periodicity in Sr/Ca records through all tridacnids in this study. This daily
631 periodicity may be caused by the ctenidium in tridacnids working in a daily rhythm to keep the
632 acid-base balance in the hemolymph of the clams to offset the CO_2 depletion by photosymbionts
633 (which is paced to the day-night cycle of light availability). In the process, Ca^{2+}-channels and
634 Na^{+}/H^{+}-exchangers work to keep the charge balance in the internal fluid and provide nutrients and
635 ions for shell mineralization, letting in compatible trace elements such as Sr^{2+} (Ip and Chew,
636 2021). This mechanism follows the biomineralization model by Carré et al. (2006) and is

supported by the high affinity of Sr^{2+} with Ca-channels (Hagiwara and Byerly, 1981) and the high ionic fluxes supported by this pathway, allowing enough membrane permeability to support the fast shell formation in tridacnids (Coimbra et al., 1988; Sather and McCleskey, 2003). Following this line of reasoning, the preconcentration of Sr^{2+} in the extrapallial fluid by Ca-channels should have a larger effect on shell Sr/Ca ratios in tridacnids than the discrimination against Sr^{2+} (or other trace elements) by the shell organic matrix during mineralization of the shell from this fluid (as proposed in Gillikin et al. (2005). This model could explain the indirect link between trace element incorporation into the shell of tridacnids and the day-night cycle without a direct causal relationship between trace element concentration and light availability (as demonstrated by the strong daily cycle in trace elements in the shaded **TSM1** specimen). It is worth noting that experiments on freshwater bivalves (e.g., *Corbicula fluminea*; Zhao et al., 2017) revealed that a closure of the Ca^{2+} channels did not influence Sr concentrations in the shell, arguing against a kinetic effect on Sr partitioning into the shell.

4.3.3 Tidal vs. diurnal variability

Our spectral analysis does not allow us to distinguish between the expression of the solar day (24 h) and lunar day (~24.8 h) because the width of the bandpass filters used to extract periodicities (~22–36 h) encompass both frequencies. While we cannot exclude the possibility that some of the daily (24 h frequency band) periodicity in tridacnid records is an expression of the lunar cycle, it seems unlikely for most records except Sr/Ca, because the expression of the other lunar periodicities (most notably the ~12 h cycle) is much weaker in tridacnids compared to the pectinids (see **Fig. 6-7**). Nevertheless, it remains possible that the diurnal cycle in Sr/Ca in tridacnids, previously interpreted as a response to the day-night cycle, is in fact caused by a circadian rhythm paced to the lunar day. Additionally, vertical mixing, a major driver of sea surface temperature changes in the northern Gulf of Aqaba, is shown to be driven by a combination of surface wind intensity (which has strong daily variability) and the presence of tidal currents (Carlson et al.,

2014). It is therefore possible that changes in local surface water temperature partly control the observed (semi-)diurnal variability in trace element concentrations in Red Sea tridacnids.

4.3.4 Seasonal variability and temperature relationships

On longer (seasonal) timescales, Sr/Ca in tridacnids has been suggested as a temperature proxy similar to the well-known Sr/Ca-Sea Surface Temperature relationship in tropical corals (Lough, 2010; Yan et al., 2013). However, significantly lower Sr/Ca ratios in tridacnids compared to coral aragonite (1.5 – 2.0 mmol mol^{-1} vs. 7.5 – 9.5 mmol mol^{-1} in corals; Elliot et al., 2009; **Fig. 2**) suggest that tridacnids exert a large degree of biological control on the Sr concentration in their shells, either through the light-sensitive photosymbiosis-calcification relationship outlined above (**section 4.3.2**) or otherwise through active Sr removal from the biomineralization site by Sr-binding organic molecules (following the model proposed by Gillikin et al., 2005). Similarly, Mg/Ca ratios in tridacnids were previously thought to primarily record water temperature (e.g., Batenburg et al., 2011) but our detailed investigation shows large differences in Mg concentration within tridacnid shells and a strong anticorrelation of Mg with sulfur compounds associated with the organic matrix in the shell (see **section 4.2.1**; Dauphin et al., 2003), has been put forward as evidence for a strong control of calcification and microstructure on Mg composition in tridacnid shells (Yoshimura et al., 2014). However, evidence from studies on foraminifera calcification demonstrate that the sulfur in biogenic carbonates is not organically bound and that the covariation with Mg might instead be caused by lattice distortion due to incorporation of Mg favoring simultaneous S incorporation (van Dijk et al., 2017). If this is also the case in tridacnids, the Mg/Ca-S/Ca covariance observed in previous studies might not preclude the use of Mg/Ca as a temperature proxy. In that case, more detailed calibration studies (e.g. using controlled growth experiments; Warter et al., 2018) are required to establish this proxy.

4.3.5 Ba/Ca and Mn/Ca in tridacnids

As in the pectinids, Ba/Ca ratios in tridacnids likely reflect changes in Ba concentration in the environment, which can be caused by upwelling of comparatively nutrient-rich waters or blooms of Ba-rich phytoplankton (Vander Putten et al., 2000; Elliot et al., 2009). Given that Mn is mostly associated with the mineral fraction of bivalve shells and seems to fractionate into the shell close to equilibrium with seawater (Onuma et al., 1979; Soldati et al., 2016), Mn/Ca ratios in tridacnids likely reflect the availability of dissolved Mn in the water column, as in other mollusk taxa (e.g., Barats et al., 2009; see **section 4.2**). This assumption is supported by the correlation between Mn/Ca and Ba/Ca measured in this study (**Fig. 2**), suggesting that both records are influenced on seasonal timescales by variability in nutrient availability and redox conditions (*sensu* Dehairs et al., 1989). Part of this correlation between Mn/Ca and Ba/Ca is driven by synchronous increases in both elements near the start and end of the profiles through tridacnid shells (**Fig. 2**). These changes may reflect a decrease of control on shell composition during periods of stress, or alternatively reflect periods of slower growth which cause more primitive microstructures (characterized by higher concentrations of trace elements) to be formed (Warter et al., 2018).

4.2.6 Environmental changes in the Gulf of Aqaba

Given that the Gulf of Aqaba is oligotrophic, seasonally stratified, and lacks significant riverine inputs (Nassar et al., 2014; Manasrah et al., 2019), the variability in nutrient concentrations and redox conditions driving Mn/Ca and Ba/Ca variability in tridacnids is likely predominantly driven by convective overturning. The tidal amplitude is much smaller than in the Bay of Brest (< 1 m; Manasrah et al., 2019) and is unlikely to drive significant short-term fluctuations in sea water chemistry. This may explain the lack of tidal (12 h) periodicity in Ba/Ca and Mn/Ca in tridacnids (**Fig. 5-6**). Nevertheless, tidal rhythms have been observed in the behavior and growth of deep-sea bivalves living far below the direct influence of tides on the environment, proving that such patterns can be recorded by the animals through their circadian rhythm (Schöne and Giere, 2005; Nedoncelle et al., 2013; Mat et al., 2020). In this case, the daily cycle seems to have been more

important for Ba/Ca in tridacnids, plausibly by driving diurnal changes in primary productivity in the Gulf of Aqaba. Alternatively, the daily periodicity found in tridacnid shell chemistry could be a response to the lunar day (~24.8 h) cycle, which is imprinted in the shell's chemical composition through periodic exposure of the clams to extreme heat or air (subaerial exposure) in their shallow water environment during exceptionally low tides. The stress induced from this exposure could have affected calcification and incorporation of trace elements (see **section 4.3.5**).

Interestingly, Sr/Ca ratios in tridacnids do exhibit tidal periodicity (**Table 2**; **Fig. 3**), perhaps driven by a circadian rhythm in calcification linked to the tidal cycle, or by subtle changes in water temperature driven by tidal currents (Carlson et al., 2014). This 12 h periodic behavior is not observed in previous studies of Sr/Ca ratios in tridacnids (Sano et al., 2012; Warter et al., 2018). A recent valvometric study on tridacnids found a 12 h period in activity, which supports the hypothesis that a circadian rhythm paced to the tidal cycle could influence shell calcification (Killam et al., 2023) . Significant daily fluctuations in solar radiation (up to 1500 W m^{-2}; (Manasrah et al., 2019)) likely exert control on the calcification of tridacnids in the Red Sea, explaining the strong diurnal periodicity in Sr/Ca and Ba/Ca records in this study (see **Fig. 6** and **Fig. 8**). As in the (non-symbiotic) pectinids, it seems likely that the majority of Mn/Ca and Ba/Ca variability in tridacnids directly reflects changes in the chemistry of the sea water and its constituents (e.g., particulate organic matter) while Mg/Ca and Sr/Ca variations are driven by changes in calcification and microstructure. The latter may be indirectly influenced by light intensity through photosynthesis by the symbionts, or by circadian rhythms paces to the diurnal or tidal cycle.

4.4 Role of photosymbiosis on high-frequency chemical variability

4.4.1 Effect of symbiosis on shell formation

While the amplitude of diurnal variability in trace element concentrations does not vary much between the symbiotic tridacnids and the non-symbiotic pectinids (**Fig. 6**), the amount of variance in the trace element records explained by daily cyclicity is up to twice as high in tridacnids (**Fig. 7**; **Table 3**). This suggests that the 24 h cycle has a much larger relative influence on trace element composition (especially Sr/Ca and Ba/Ca) in tridacnids than in pectinids. This seems to point towards a role of the photosymbionts in calcification by tridacnids, such as through symbiont-mediated diurnal variation in the pH of the extrapallial fluid (Ip et al., 2006), as well as active transport of HCO_3^- for calcification (Chew et al., 2019) and as a C supply to the symbionts from the host (Boo et al., 2021). Given the differences in elemental ratios between these two groups of bivalves, comparing variance yields a more robust assessment of the relative importance of tidal or diurnal variability on shell composition than looking at the absolute size (amplitude) of the chemical cycle. While the difference in variance is clear, the importance of diurnal cyclicity on the photosymbiotic tridacnids is not as big as one might expect. Rarely more than 10 % of the variance is explained by day-night variability (**Table 3**). This seems to contradict the large daily Sr/Ca amplitudes found in Warter et al. (2018) and the trace element fluctuations found in de Winter et al. (2020), which rival the seasonal cycle in these trace element ratios in terms of amplitude. However, the percentages in **Table 3** relate to the amount of variation in the complete records through these individuals and therefore also contain areas of the shell where daily cyclicity is less pronounced, while values in previous studies often reflect maximum amplitudes recorded in parts of the shell with exceptionally clear daily increments.

4.4.2 Effect of differences in the environment

It seems plausible that part of the difference in diurnal variability between pectinids and tridacnids is explained by a difference in the environment between the Gulf of Aqaba and the Bay of Brest, rather than the presence of photosymbionts. The diurnal insolation cycle in the Gulf of Aqaba is larger than in the Bay of Brest (1500 vs 546 W m^{-2} maximum summer irradiance, respectively;

Roberts et al., 2018; Manasrah et al., 2019). If calcification in pectinids would be equally sensitive to sunlight, this difference may explain much of the difference between the species. In this scenario, part of the strong tidal component in the pectinid trace element data may be explained by the influence of differences in water depth on the penetration of sunlight through the murky waters of the Bay of Brest (Roberts et al., 2018). Tidal movement can cause strong non-linear amplification or reduction of the solar irradiance at the sea floor of the Bay of Brest by factors exceeding 10, especially outside the summer months, which in turn has a significant effect on primary productivity in the water column (Roberts et al., 2018). This tidal effect is likely to be much weaker in the Gulf of Aqaba, given its comparatively low tidal amplitude, clear oligotrophic waters, and much stronger and less seasonal day-night cycle (Manasrah et al., 2019). Indeed, even in non-photosymbiotic bivalves, light and food availability are demonstrated to be major drivers of the animal's behavior (e.g. Ballesta-Artero et al., 2017). The combination of the daily and tidal cycles on solar irradiance at depth and photosynthesis in the Bay of Brest may therefore pose an alternative pathway for strong tidal cyclicity in the trace element composition of pectinids in this study and account for part of the twofold increase in daily variability in tridacnids compared to the pectinids (**Fig. 7-8**; **Table 3**).

4.4.3 Effect of direct insolation

Specimen **TSM1** poses an interesting case study for investigating the link between sunlight and calcification in tridacnids, since it grew under a sunshade and therefore experienced a dampened diurnal variability in insolation compared to other giant clams in the area. The fact that this specimen exhibits similar or even higher diurnal variability in shell chemistry (**Fig. 7**) argues against a direct influence of the rate of photosynthesis itself on calcification. Instead, it seems that daily chemical variability is mostly an expression of circadian rhythm in tridacnids, which is strongly (evolutionarily) coupled to the day-night cycle to optimize the symbiosis with primary producers in its mantle, possibly through respiration rhythms carried out by the ctenidium (see

784 **section 4.3**; Ip and Chew, 2021). Symbionts have been shown to directly aid in calcification
785 through proton pumping (Armstrong et al., 2018), influencing internal acid-base chemistry (Ip et
786 al., 2006), and valvometric studies show the clams bask in sunlight in daylight hours and close
787 partially at night when symbiosis is likely reduced (Schwartzmann et al., 2011, Killam et al., 2023).
788 This conclusion is further supported by the lack of a clear difference in diurnal cyclicity between
789 trace element records in *T. maxima*, *T. squamosa* and *T. squamosina* (**Fig. 7**; **Table 3**), even
790 though the degree of reliance on photosymbiosis is demonstrated to be highly variable between
791 these species (Killam et al., 2020). Therefore, it seems unlikely that sub-daily resolved trace
792 element records in tridacnids can be used as quantitative recorders of paleo-insolation, as was
793 originally suggested by Sano et al. (2012). While the degree of symbiotic activity may not be
794 clearly recorded in the daily amplitude of trace element oscillations, the consistency of daily
795 periodic signal in the studied giant clams could relate to the direct biological control exerted by
796 the symbionts on the hosts' rhythms of calcification. Light exposure in giant clams promotes
797 expression of genes coding for proteins involved in Ca^{2+}, H^{+} and HCO_3^{-} transport in the mantles
798 of giant clams (Ip et al., 2017; Chew et al., 2019), with the expression proposed to be at least
799 partially mediated by photosensing on the part of the symbionts themselves (Ip et al., 2017).
800 Differences between the daily consistency (spectral power) of photosymbiotic and non-
801 photosymbiotic trace element profiles might still allow paleontologists to use the presence of
802 strong daily periodicity as a proxy for photosymbiosis in the fossil record (as suggested by de
803 Winter et al. (2020). However, the small differences found between pectinids and tridacnids in
804 this study and the comparatively large influence of environmental variability show that such
805 records should be interpreted with caution. Future studies could measure photosynthetic activity
806 of the symbionts in tridacnids and attempt to relate this to the trace element composition of the
807 shell to isolate the direct effect of photosymbiosis on shell composition.

808

4.5 Aperiodic drivers of shell chemistry

4.5.1 Circadian and behavioral changes

Even after controlling for instrumental noise, most (~ 90 %) of the variance observed in our trace element records is not directly related to the diurnal or tidal cycle. This suggests that aperiodic events at the scale of hours to days play an important role in the calcification of pectinids and tridacnids. Given the large difference in ecological niche (e.g., photosymbiotic versus non-symbiotic) between these taxa, and the difference between the environment in which they grew, this observation suggests that calcification of bivalves at the (sub-)daily scale is generally dominated by aperiodic variability in calcification or in the environment. Part of this unaccounted variability may be caused by variability in the animal's behavior, as documented by observations of siphon and valve gape activity in cultured or monitored specimens of a variety of bivalve taxa (Rodland et al., 2006; Ballesta-Artero et al., 2017). While these experiments revealed quasi-periodic (3-7 minute and 60–90 minute periods) behavior unassociated with the tidal or daily cycle, records of activity of the bivalves also reveal less regular patterns on the scale of 2–24 h which may contribute to the aperiodic variance in trace element records (Rodland et al., 2006). Another example of aperiodic behavior potentially influencing shell chemistry is rapid valve adduction or "coughing" observed in both pectinids and tridacnids, which serves as a mechanism for expelling respiratory CO_2 and faeces from the pallial cavity or to evade predation attempts (Robson et al., 2012; Soo and Todd, 2014). This behavior could resuspend sediment and produce pulses of Mn and Ba at the sediment-water interface which are recorded as short-term, aperiodic variability in these elements in the shell. The temporal sampling resolution (several hours) of our trace element records after smoothing out measurement noise does not allow us to resolve the types of periodic variability at the sub-hourly scale cited in these previous studies, meaning that aperiodic variability in behavior and aliasing of these ultradian patterns likely contribute to the aperiodic variability in our trace element records. On longer (sub-)seasonal timescales, activity in bivalves is shown to

be highly dependent on food and light availability (Ballesta-Artero et al., 2017), suggesting that aperiodic, short-term changes in these environmental factors could be a main driver of shell growth and composition and explain a large part of the variance in the trace element records which is not explained by ultradian changes in the animal's behavior.

4.5.2 Short-term environmental changes and paleoweather

Outside of regular fluctuations caused by tidal, daily, and seasonal cycles, changes in light and food availability at the hourly to daily scale are probably linked to circulation and weather phenomena. Previous studies show that enhanced vertical mixing during weather events such as storms, algal bloom events after wind-driven upwelling and pseudoperiodic dust deposition can temporarily increase the concentration of dissolved metals in surface waters, resuspend organic matter and temporarily increase primary productivity (Lin et al., 2003; Al-Najjar et al., 2007; Iluz et al., 2009; Al-Taani et al., 2015; Komagoe et al., 2018). This will in turn lead to a shallowing of the redoxcline through increased organic matter load at the sediment-water interface, which can be recorded in the composition of giant clam shells (Yan et al., 2020). Interestingly, data in Yan et al. (2020) suggest that recording an extreme weather event in *Tridacna* requires wind speeds exceeding 20 km/h, a threshold which is almost never reached in the comparatively quiet Gulf of Aqaba (Manasrah et al., 2019), while such events are common in the stormier Bay of Brest (Hily et al., 1992; Chauvaud et al., 2005). This difference is also reflected in the periodicity of shell composition, with the tridacnids having overall higher percentages of their variance explained by daily and tidal variability than pectinids (**Fig. 3 and 7**), showing that aperiodic (potentially weather-controlled) variability in shell composition has a stronger influence on the pectinids which grew in the stormier Bay of Brest. A plausible scenario therefore emerges in which aperiodic weather events cause short-term variability in both the chemistry and physical properties of the water column. These changes are subsequently recorded in bivalve shells, either directly because the weather events resuspend, remobilize or deliver trace elements like Mn and Ba (e.g., Dehairs et

al., 1989; Gillikin et al., 2008; Mahé et al., 2010), or indirectly because environmental stress associated with the event affects behavior and shell calcification, resulting in a change in the incorporation of alkali-group cations (e.g., Mg and Sr) into the shell biomineral (Carré et al., 2006; Takesue et al., 2008; **Fig. 8**). Our results therefore highlight the potential of high-resolution trace element records in bivalve shells to record short-term circulation changes and weather events, while prescribing caution in interpreting such records until the effect of true environmental changes on the sub-daily scale can be separated from aperiodic ultradian or behavioral patterns.

5. Conclusions

Our high-resolution trace element records reveal that short-term variability on the tidal and daily scale is recorded in the Mg, Sr, Mn, and Ba composition of shells of fast-growing mollusk species. The application of spectral analysis and variance decomposition on these trace element records is a useful tool to assess the influence of periodicity in the shallow marine environment on calcification in mollusk shells. Our statistical analysis reveals that tidal and daily variability on average account for less than 10 % of trace element variance in pectinids and tridacnids. In photosymbiotic giant clam shells, the amount of variance in Sr and Ba paced to the daily cycle is two times higher than in the non-photosymbiotic pectinids, suggesting that photosymbiosis in giant clams exerts some control on trace element composition in their shells. However, since only ~10 % of the trace element variability in tridacnids is explained by diurnal variability, the recognition of photosymbiosis in the fossil record from diurnal variability in fossil shell composition will be complicated. In addition, differences between the mid-latitude environment of the pectinids and the tropical environment of the tridacnids likely account for part of the difference in trace element composition between the taxa.

We propose that Ba and Mn composition in pectinids and tridacnids reflect short-term variability in primary productivity and sea water chemistry which control the mobility of these elements. Concentrations of Mg and Sr are likely controlled by short-term changes in growth and metabolic rate of the mollusks, which may be indirectly controlled by changes in their environment through circadian rhythms or behavior, explaining the pacing of trace element composition to the tidal and diurnal cycle. Most of the variance in trace element records in both taxa are not related to periodic behavior at the 12 h or 24 h scale, likely recording aperiodic events in the environment related to weather-scale phenomena or circadian patterns. We thus conclude that mollusk shell carbonate is a promising archive for recording weather-scale variability in shallow marine environments

891 across latitudes, potentially recording weather-scale phenomena in deep time, as long as these
892 environmental effects can be separated by the influence of the behavior of the animal.

893

894 **Code availability**

895 Scripts used for data processing and to create figures in this manuscript were uploaded to an
896 open-access repository on GitHub (https://github.com/nielsjdewinter/TE_circadian) and linked
897 through Zenodo (https://zenodo.org/record/6603175).

898

899 **Data availability**

900 Supplementary data and figures referenced in this contribution were uploaded to the online open-
901 access repository Zenodo (https://doi.org/10.5281/zenodo.6602894).

902

903 **Author contribution**

904 NJW designed the experiment after discussion with BRS, DK and LF. LF, DK, BRS and JT
905 collected the samples. LF, DK and NJW together prepared samples for analyses and constructed
906 shell chronologies using growth line counting. WB, LN, GJR and NJW carried out the LA-ICP-MS
907 analyses and data processing. NJW designed and carried out the statistical analyses and wrote
908 the R scripts guided by feedback from LF, BK, LN, WB and GJR. NJW wrote the first draft of the
909 manuscript. All authors contributed to the writing process towards the final version of the
910 manuscript.

911

912 **Competing interests**

The authors declare that they have no conflict of interest.

Acknowledgements

The authors would like to thank Leonard Bik for his help with sample preparation and Maarten Zeilmans for his help with high-resolution imaging of the samples at Utrecht University. This study is part of the UNBIAS project, jointly funded by a Flemish Research Foundation (FWO; 12ZB220N) post-doctoral fellowship (NJW) and a MSCA Individual Fellowship (H2020-MSCA-IF-2018; 843011 – UNBIAS; awarded to NJW). GJR and LKD acknowledge funding from the Netherlands Earth System Science Center (NESSC; grant no. 024.002.001) from the Dutch Ministry for Education, Culture and Science (gravitation grant no. NWO 024.002.001). BRS acknowledges funding from the Deutsche Forschungsgemeinschaft (DFG; SCHO 793/21 [HIPPO]+ SCHO 793/23). JT acknowledges funding from the French National Research Agency (ANR; ANR-18-CE92-0036-01) awarded within the framework of the French-German collaborative project HIPPO (HIgh-resolution Primary Production multiprOxy archives).

References

Agbaje, O. B. A., Wirth, R., Morales, L. F. G., Shirai, K., Kosnik, M., Watanabe, T., and Jacob, D. E.: Architecture of crossed-lamellar bivalve shells: the southern giant clam (Tridacna derasa, Röding, 1798), R. Soc. Open Sci., 4, 170622, https://doi.org/10.1098/rsos.170622, 2017.

Al-Aasm, I. S. and Veizer, J.: Diagenetic stabilization of aragonite and low-Mg calcite, I. Trace elements in rudists, J. Sediment. Res., 56, 138–152, 1986a.

Al-Aasm, I. S. and Veizer, J.: Diagenetic stabilization of aragonite and low-Mg calcite, II. Stable isotopes in rudists, J. Sediment. Res., 56, 1986b.

Al-Najjar, T., Badran, M. I., Richter, C., Meyerhoefer, M., and Sommer, U.: Seasonal dynamics of phytoplankton in the Gulf of Aqaba, Red Sea, Hydrobiologia, 579, 69–83, https://doi.org/10.1007/s10750-006-0365-z, 2007.

Al-Taani, A. A., Rashdan, M., and Khashashneh, S.: Atmospheric dry deposition of mineral dust to the Gulf of Aqaba, Red Sea: Rate and trace elements, Mar. Pollut. Bull., 92, 252–258, https://doi.org/10.1016/j.marpolbul.2014.11.047, 2015.

941 Anand, P. and Elderfield, H.: Variability of Mg/Ca and Sr/Ca between and within the planktonic
942 foraminifers Globigerina bulloides and Globorotalia truncatulinoides, Geochem. Geophys. Geosystems,
943 6, https://doi.org/10.1029/2004GC000811, 2005.

944 Armstrong, E. J., Roa, J. N., Stillman, J. H., and Tresguerres, M.: Symbiont photosynthesis in giant clams is
945 promoted by V-type H+-ATPase from host cells, J. Exp. Biol., 221, jeb177220,
946 https://doi.org/10.1242/jeb.177220, 2018.

947 Ballesta-Artero, I., Witbaard, R., Carroll, M. L., and van der Meer, J.: Environmental factors regulating
948 gaping activity of the bivalve Arctica islandica in Northern Norway, Mar. Biol., 164, 116, 2017.

949 Barats, A., Amouroux, D., Pécheyran, C., Chauvaud, L., and Donard, O. F. X.: High-Frequency Archives of
950 Manganese Inputs To Coastal Waters (Bay of Seine, France) Resolved by the LA−ICP−MS Analysis of
951 Calcitic Growth Layers along Scallop Shells (Pecten maximus), Environ. Sci. Technol., 42, 86–92,
952 https://doi.org/10.1021/es0701210, 2008.

953 Barats, A., Amouroux, D., Chauvaud, L., Pécheyran, C., Lorrain, A., Thébault, J., Church, T. M., and
954 Donard, O. F. X.: High frequency Barium profiles in shells of the Great Scallop *Pecten maximus*: a
955 methodical long-term and multi-site survey in Western Europe, Biogeosciences, 6, 157–170,
956 https://doi.org/10.5194/bg-6-157-2009, 2009.

957 Batenburg, S. J., Reichart, G.-J., Jilbert, T., Janse, M., Wesselingh, F. P., and Renema, W.: Interannual
958 climate variability in the Miocene: High resolution trace element and stable isotope ratios in giant clams,
959 Palaeogeogr. Palaeoclimatol. Palaeoecol., 306, 75–81, 2011.

960 Black, B. A.: Climate-driven synchrony across tree, bivalve, and rockfish growth-increment chronologies
961 of the northeast Pacific, Mar. Ecol. Prog. Ser., 378, 37–46, 2009.

962 Boo, M. V., Chew, S. F., and Ip, Y. K.: The colorful mantle of the giant clam Tridacna squamosa expresses
963 a homolog of electrogenic sodium: Bicarbonate cotransporter 2 that mediates the supply of inorganic
964 carbon to photosynthesizing symbionts, PloS One, 16, e0258519,
965 https://doi.org/10.1371/journal.pone.0258519, 2021.

966 Bougeois, L., De Rafélis, M., Reichart, G.-J., De Nooijer, L. J., Nicollin, F., and Dupont-Nivet, G.: A high
967 resolution study of trace elements and stable isotopes in oyster shells to estimate Central Asian Middle
968 Eocene seasonality, Chem. Geol., 363, 200–212, 2014.

969 Carlson, D. F., Fredj, E., and Gildor, H.: The annual cycle of vertical mixing and restratification in the
970 Northern Gulf of Eilat/Aqaba (Red Sea) based on high temporal and vertical resolution observations,
971 Deep Sea Res. Part Oceanogr. Res. Pap., 84, 1–17, https://doi.org/10.1016/j.dsr.2013.10.004, 2014.

972 Carré, M., Bentaleb, I., Bruguier, O., Ordinola, E., Barrett, N. T., and Fontugne, M.: Calcification rate
973 influence on trace element concentrations in aragonitic bivalve shells: Evidences and mechanisms,
974 Geochim. Cosmochim. Acta, 70, 4906–4920, https://doi.org/10.1016/j.gca.2006.07.019, 2006.

975 Chauvaud, L., Lorrain, A., Dunbar, R. B., Paulet, Y.-M., Thouzeau, G., Jean, F., Guarini, J.-M., and
976 Mucciarone, D.: Shell of the Great Scallop Pecten maximus as a high-frequency archive of
977 paleoenvironmental changes, Geochem. Geophys. Geosystems, 6, 2005.

978 Checa, A. G., Esteban-Delgado, F. J., and Rodríguez-Navarro, A. B.: Crystallographic structure of the
979 foliated calcite of bivalves, J. Struct. Biol., 157, 393–402, 2007.

980 Chew, S. F., Koh, C. Z., Hiong, K. C., Choo, C. Y., Wong, W. P., Neo, M. L., and Ip, Y. K.: Light-enhanced
981 expression of Carbonic Anhydrase 4-like supports shell formation in the fluted giant clam Tridacna
982 squamosa, Gene, 683, 101–112, 2019.

983 Cochran, J. K., Kallenberg, K., Landman, N. H., Harries, P. J., Weinreb, D., Turekian, K. K., Beck, A. J., and
984 Cobban, W. A.: Effect of diagenesis on the Sr, O, and C isotope composition of late Cretaceous mollusks
985 from the Western Interior Seaway of North America, Am. J. Sci., 310, 69–88,
986 https://doi.org/10.2475/02.2010.01, 2010.

987 Cohen, A. L., Owens, K. E., Layne, G. D., and Shimizu, N.: The Effect of Algal Symbionts on the Accuracy of
988 Sr/Ca Paleotemperatures from Coral, Science, 296, 331–333, https://doi.org/10.1126/science.1069330,
989 2002.

990 Coimbra, J., Machado, J., Fernandes, P. L., Ferreira, H. G., and Ferreira, K. G.: Electrophysiology of the
991 Mantle of Anodonta Cygnea, J. Exp. Biol., 140, 65–88, https://doi.org/10.1242/jeb.140.1.65, 1988.

992 Coimbra, R., Huck, S., de Winter, N. J., Heimhofer, U., and Claeys, P.: Improving the detection of shell
993 alteration: Implications for sclerochronology, Palaeogeogr. Palaeoclimatol. Palaeoecol., 559, 109968,
994 https://doi.org/10.1016/j.palaeo.2020.109968, 2020.

995 Comboul, M., Emile-Geay, J., Evans, M. N., Mirnateghi, N., Cobb, K. M., and Thompson, D. M.: A
996 probabilistic model of chronological errors in layer-counted climate proxies: applications to annually
997 banded coral archives, Clim. Past, 10, 825–841, 2014.

998 Crippa, G., Griesshaber, E., Checa, A. G., Harper, E. M., Roda, M. S., and Schmahl, W. W.: Orientation
999 patterns of aragonitic crossed-lamellar, fibrous prismatic and myostracal microstructures of modern
1000 Glycymeris shells, J. Struct. Biol., 212, 107653, 2020.

1001 Dauphin, Y., Cuif, J., Doucet, J., Salomé, M., Susini, J., and Williams, C.: In situ mapping of growth lines in
1002 the calcitic prismatic layers of mollusc shells using X-ray absorption near-edge structure (XANES)
1003 spectroscopy at the sulphur K-edge, Mar. Biol., 142, 299–304, 2003.

1004 Day, C. C. and Henderson, G. M.: Controls on trace-element partitioning in cave-analogue calcite,
1005 Geochim. Cosmochim. Acta, 120, 612–627, https://doi.org/10.1016/j.gca.2013.05.044, 2013.

1006 DeCarlo, T. M. and Cohen, A. L.: Dissepiments, density bands and signatures of thermal stress in Porites
1007 skeletons, Coral Reefs, 36, 749–761, https://doi.org/10.1007/s00338-017-1566-9, 2017.

1008 Dehairs, F., Baeyens, W., and Van Gansbeke, D.: Tight coupling between enrichment of iron and
1009 manganese in North Sea suspended matter and sedimentary redox processes: Evidence for seasonal
1010 variability, Estuar. Coast. Shelf Sci., 29, 457–471, https://doi.org/10.1016/0272-7714(89)90080-2, 1989.

1011 van Dijk, I., de Nooijer, L. J., Boer, W., and Reichart, G.-J.: Sulfur in foraminiferal calcite as a potential
1012 proxy for seawater carbonate ion concentration, Earth Planet. Sci. Lett., 470, 64–72, 2017.

Dunbar, R. B. and Wellington, G. M.: Stable isotopes in a branching coral monitor seasonal temperature variation, Nature, 293, 453–455, 1981.

Eggins, S., De Deckker, P., and Marshall, J.: Mg/Ca variation in planktonic foraminifera tests: implications for reconstructing palaeo-seawater temperature and habitat migration, Earth Planet. Sci. Lett., 212, 291–306, https://doi.org/10.1016/S0012-821X(03)00283-8, 2003.

Elliot, M., Welsh, K., Chilcott, C., McCulloch, M., Chappell, J., and Ayling, B.: Profiles of trace elements and stable isotopes derived from giant long-lived Tridacna gigas bivalves: potential applications in paleoclimate studies, Palaeogeogr. Palaeoclimatol. Palaeoecol., 280, 132–142, 2009.

Freitas, P. S., Clarke, L. J., Kennedy, H., Richardson, C. A., and others: Ion microprobe assessment of the heterogeneity of Mg/Ca, Sr/Ca and Mn/Ca ratios in Pecten maximus and Mytilus edulis (bivalvia) shell calcite precipitated at constant temperature, Biogeosciences Discuss., 6, 1267, 2009.

Fröhlich, L., Siebert, V., Walliser, E. O., Thébault, J., Jochum, K. P., Chauvaud, L., and Schöne, B. R.: Ba/Ca profiles in shells of Pecten maximus – A proxy for specific primary producers rather than bulk phytoplankton, Chem. Geol., 120743, https://doi.org/10.1016/j.chemgeo.2022.120743, 2022.

Gannon, M. E., Pérez-Huerta, A., Aharon, P., and Street, S. C.: A biomineralization study of the Indo-Pacific giant clam Tridacna gigas, Coral Reefs, 36, 503–517, https://doi.org/10.1007/s00338-016-1538-5, 2017.

García-March, J. R., Sanchís Solsona, M. Á., and García-Carrascosa, A. M.: Shell gaping behaviour of Pinna nobilis L., 1758: circadian and circalunar rhythms revealed by in situ monitoring, Mar. Biol., 153, 689–698, https://doi.org/10.1007/s00227-007-0842-6, 2008.

Gilbert, P. U., Bergmann, K. D., Myers, C. E., Marcus, M. A., DeVol, R. T., Sun, C.-Y., Blonsky, A. Z., Tamre, E., Zhao, J., and Karan, E. A.: Nacre tablet thickness records formation temperature in modern and fossil shells, Earth Planet. Sci. Lett., 460, 281–292, 2017.

Gillikin, D. P., Lorrain, A., Navez, J., Taylor, J. W., André, L., Keppens, E., Baeyens, W., and Dehairs, F.: Strong biological controls on Sr/Ca ratios in aragonitic marine bivalve shells, Geochem. Geophys. Geosystems, 6, https://doi.org/10.1029/2004GC000874, 2005.

Gillikin, D. P., Lorrain, A., Paulet, Y.-M., André, L., and Dehairs, F.: Synchronous barium peaks in high-resolution profiles of calcite and aragonite marine bivalve shells, Geo-Mar. Lett., 28, 351–358, 2008.

Goodwin, D. H., Paul, P., and Wissink, C. L.: MoGroFunGen: A numerical model for reconstructing intra-annual growth rates of bivalve molluscs, Palaeogeogr. Palaeoclimatol. Palaeoecol., 276, 47–55, https://doi.org/10.1016/j.palaeo.2009.02.026, 2009.

Guillaume Olivier, M., Leroux, E., Rabineau, M., Le Hir, P., Granjeon, D., Chataigner, T., Beudin, A., and Muller, H.: Numerical modelling of a Macrotidal Bay over the last 9,000 years: An interdisciplinary methodology to understand the influence of sea-level variations on tidal currents in the Bay of Brest, Cont. Shelf Res., 231, 104595, https://doi.org/10.1016/j.csr.2021.104595, 2021.

Guillong, M., Meier, D. L., Allan, M. M., Heinrich, C. A., and Yardley, B. W. D.: SILLS: A Matlab-based program for the reduction of laser ablation ICP–MS data of homogenous materials and inclusions, Mineral. Assoc. Can. Short Course, 40, 328–333, 2008.

Hagiwara, S. and Byerly, L.: Calcium channel, Annu. Rev. Neurosci., 4, 69–125, 1981.

Hallmann, N., Schöne, B. R., Strom, A., and Fiebig, J.: An intractable climate archive—Sclerochronological and shell oxygen isotope analyses of the Pacific geoduck, Panopea abrupta (bivalve mollusk) from Protection Island (Washington State, USA), Palaeogeogr. Palaeoclimatol. Palaeoecol., 269, 115–126, 2008.

Hily, C., Potin, P., and Floc'h, J.-Y.: Structure of subtidal algal assemblages on soft-bottom sediments: fauna/flora interactions and role of disburbances in the Bay of Brest, France, Mar. Ecol. Prog. Ser., 85, 115–130, 1992.

Höche, N., Peharda, M., Walliser, E. O., and Schöne, B. R.: Morphological variations of crossed-lamellar ultrastructures of Glycymeris bimaculata (Bivalvia) serve as a marine temperature proxy, Estuar. Coast. Shelf Sci., 237, 106658, https://doi.org/10.1016/j.ecss.2020.106658, 2020.

Höche, N., Walliser, E. O., de Winter, N. J., Witbaard, R., and Schöne, B. R.: Temperature-induced microstructural changes in shells of laboratory-grown Arctica islandica (Bivalvia), PloS One, 16, e0247968, 2021.

Huyghe, D., de Rafelis, M., Ropert, M., Mouchi, V., Emmanuel, L., Renard, M., and Lartaud, F.: New insights into oyster high-resolution hinge growth patterns, Mar. Biol., 166, 48, 2019.

Huyghe, D., Daëron, M., de Rafelis, M., Blamart, D., Sébilo, M., Paulet, Y.-M., and Lartaud, F.: Clumped isotopes in modern marine bivalves, Geochim. Cosmochim. Acta, 316, 41–58, https://doi.org/10.1016/j.gca.2021.09.019, 2021.

Iluz, D., Dishon, G., Capuzzo, E., Meeder, E., Astoreca, R., Montecino, V., Znachor, P., Ediger, D., and Marra, J.: Short-term variability in primary productivity during a wind-driven diatom bloom in the Gulf of Eilat (Aqaba), Aquat. Microb. Ecol., 56, 205–215, https://doi.org/10.3354/ame01321, 2009.

Inoue, M., Nakamura, T., Tanaka, Y., Suzuki, A., Yokoyama, Y., Kawahata, H., Sakai, K., and Gussone, N.: A simple role of coral-algal symbiosis in coral calcification based on multiple geochemical tracers, Geochim. Cosmochim. Acta, 235, 76–88, https://doi.org/10.1016/j.gca.2018.05.016, 2018.

Ip, Y. K. and Chew, S. F.: Light-Dependent Phenomena and Related Molecular Mechanisms in Giant Clam-Dinoflagellate Associations: A Review, Front. Mar. Sci., 8, 2021.

Ip, Y. K., Loong, A. M., Hiong, K. C., Wong, W. P., Chew, S. F., Reddy, K., Sivaloganathan, B., and Ballantyne, J. S.: Light induces an increase in the pH of and a decrease in the ammonia concentration in the extrapallial fluid of the giant clam Tridacna squamosa, Physiol. Biochem. Zool., 79, 656–664, 2006.

Ip, Y. K., Koh, C. Z., Hiong, K. C., Choo, C. Y., Boo, M. V., Wong, W. P., Neo, M. L., and Chew, S. F.: Carbonic anhydrase 2-like in the giant clam, Tridacna squamosa: characterization, localization, response to light, and possible role in the transport of inorganic carbon from the host to its symbionts, Physiol. Rep., 5, e13494, 2017.

Ivany, L. C.: Reconstructing paleoseasonality from accretionary skeletal carbonates—challenges and opportunities, Paleontol. Soc. Pap., 18, 133–166, 2012.

Ivany, L. C. and Judd, E. J.: Deciphering Temperature Seasonality in Earth's Ancient Oceans, Annu. Rev. Earth Planet. Sci., 50, 123–152, https://doi.org/10.1146/annurev-earth-032320-095156, 2022.

Jablonski, D., Roy, K., Valentine, J. W., Price, R. M., and Anderson, P. S.: The Impact of the Pull of the Recent on the History of Marine Diversity, Science, 300, 1133–1135, https://doi.org/10.1126/science.1083246, 2003.

Jablonski, D., Huang, S., Roy, K., and Valentine, J. W.: Shaping the latitudinal diversity gradient: new perspectives from a synthesis of paleobiology and biogeography, Am. Nat., 189, 1–12, 2017.

Jochum, K. P., Willbold, M., Raczek, I., Stoll, B., and Herwig, K.: Chemical Characterisation of the USGS Reference Glasses GSA-1G, GSC-1G, GSD-1G, GSE-1G, BCR-2G, BHVO-2G and BIR-1G Using EPMA, ID-TIMS, ID-ICP-MS and LA-ICP-MS, Geostand. Geoanalytical Res., 29, 285–302, https://doi.org/10.1111/j.1751-908X.2005.tb00901.x, 2005.

Jochum, K. P., Weis, U., Stoll, B., Kuzmin, D., Yang, Q., Raczek, I., Jacob, D. E., Stracke, A., Birbaum, K., and Frick, D. A.: Determination of reference values for NIST SRM 610–617 glasses following ISO guidelines, Geostand. Geoanalytical Res., 35, 397–429, 2011.

Jones, D. S.: Sclerochronology: reading the record of the molluscan shell: annual growth increments in the shells of bivalve molluscs record marine climatic changes and reveal surprising longevity, Am. Sci., 71, 384–391, 1983.

Jones, D. S. and Quitmyer, I. R.: Marking Time with Bivalve Shells: Oxygen Isotopes and Season of Annual Increment Formation, PALAIOS, 11, 340–346, https://doi.org/10.2307/3515244, 1996.

Judd, E. J., Wilkinson, B. H., and Ivany, L. C.: The life and time of clams: Derivation of intra-annual growth rates from high-resolution oxygen isotope profiles, Palaeogeogr. Palaeoclimatol. Palaeoecol., 490, 70–83, 2018.

Killam, D., Thomas, R., Al-Najjar, T., and Clapham, M.: Interspecific and Intrashell Stable Isotope Variation Among the Red Sea Giant Clams, Geochem. Geophys. Geosystems, 21, e2019GC008669, https://doi.org/10.1029/2019GC008669, 2020.

Killam, D., Al-Najjar, T., and Clapham, M.: Giant clam growth in the Gulf of Aqaba is accelerated compared to fossil populations, Proc. R. Soc. B Biol. Sci., 288, 20210991, https://doi.org/10.1098/rspb.2021.0991, 2021.

Killam, D. E. and Clapham, M. E.: Identifying the ticks of bivalve shell clocks: Seasonal growth in relation to temperature and food supply, PALAIOS, 33, 228–236, https://doi.org/10.2110/palo.2017.072, 2018a.

Killam, D. E. and Clapham, M. E.: IDENTIFYING THE TICKS OF BIVALVE SHELL CLOCKS: SEASONAL GROWTH IN RELATION TO TEMPERATURE AND FOOD SUPPLY, PALAIOS, 33, 228–236, https://doi.org/10.2110/palo.2017.072, 2018b.

Killam, D., Thompson, D., Morgan, K., and Russell, M.: Giant clams as open-source, scalable reef environmental biomonitors, Plos one, 18, e0278752, 2023.

Klein, R. T., Lohmann, K. C., and Thayer, C. W.: Bivalve skeletons record sea-surface temperature and δ18O via Mg/Ca and 18O/16O ratios, Geology, 24, 415–418, 1996.

Komagoe, T., Watanabe, T., Shirai, K., Yamazaki, A., and Uematu, M.: Geochemical and Microstructural Signals in Giant Clam Tridacna maxima Recorded Typhoon Events at Okinotori Island, Japan, J. Geophys. Res. Biogeosciences, 123, 1460–1474, https://doi.org/10.1029/2017JG004082, 2018.

Kontoyannis, C. G. and Vagenas, N. V.: Calcium carbonate phase analysis using XRD and FT-Raman spectroscopy, Analyst, 125, 251–255, https://doi.org/10.1039/A908609I, 2000.

Ku, H. H.: Notes on the use of propagation of error formulas, J. Res. Natl. Bur. Stand., 70, 263–273, 1966.

Lazareth, C. E., Vander Putten, E., André, L., and Dehairs, F.: High-resolution trace element profiles in shells of the mangrove bivalve Isognomon ephippium: a record of environmental spatio-temporal variations?, Estuar. Coast. Shelf Sci., 57, 1103–1114, 2003.

Lazareth, C. E., Guzman, N., Poitrasson, F., Candaudap, F., and Ortlieb, L.: Nyctemeral variations of magnesium intake in the calcitic layer of a Chilean mollusk shell (Concholepas concholepas, Gastropoda), Geochim. Cosmochim. Acta, 71, 5369–5383, 2007.

Lazier, A. V., SMITH, J. E., RISK, M. J., and SCHWARCZ, H. P.: The skeletal structure of Desmophyllum cristagalli: the use of deep-water corals in sclerochronology, Lethaia, 32, 119–130, 1999.

Lin, I., Liu, W. T., Wu, C.-C., Wong, G. T. F., Hu, C., Chen, Z., Liang, W.-D., Yang, Y., and Liu, K.-K.: New evidence for enhanced ocean primary production triggered by tropical cyclone, Geophys. Res. Lett., 30, https://doi.org/10.1029/2003GL017141, 2003.

Lorrain, A., Gillikin, D. P., Paulet, Y.-M., Chauvaud, L., Le Mercier, A., Navez, J., and André, L.: Strong kinetic effects on Sr/Ca ratios in the calcitic bivalve Pecten maximus, Geology, 33, 965–968, 2005.

Lough, J. M.: Climate records from corals, WIREs Clim. Change, 1, 318–331, https://doi.org/10.1002/wcc.39, 2010.

Madkour, H. A.: Distribution and relationships of heavy metals in the giant clam (Tridacna maxima) and associated sediments from different sites in the Egyptian Red Sea Coast, Egyptian Journal of Aquatic Research, 31,45-59

Mahé, K., Bellamy, E., Lartaud, F., and Rafélis, M. de: Calcein and manganese experiments for marking the shell of the common cockle (Cerastoderma edule): tidal rhythm validation of increments formation, Aquat. Living Resour., 23, 239–245, https://doi.org/10.1051/alr/2010025, 2010.

Manasrah, R., Abu-Hilal, A., and Rasheed, M.: Physical and Chemical Properties of Seawater in the Gulf of Aqaba and Red Sea, in: Oceanographic and Biological Aspects of the Red Sea, edited by: Rasul, N. M. A. and Stewart, I. C. F., Springer International Publishing, Cham, 41–73, https://doi.org/10.1007/978-3-319-99417-8_3, 2019.

Marin, F. and Luquet, G.: Molluscan shell proteins, Comptes Rendus Palevol, 3, 469–492, https://doi.org/10.1016/j.crpv.2004.07.009, 2004.

Mat, A. M., Sarrazin, J., Markov, G. V., Apremont, V., Dubreuil, C., Eché, C., Fabioux, C., Klopp, C., Sarradin, P.-M., Tanguy, A., Huvet, A., and Matabos, M.: Biological rhythms in the deep-sea hydrothermal mussel Bathymodiolus azoricus, Nat. Commun., 11, 3454, https://doi.org/10.1038/s41467-020-17284-4, 2020.

Meibom, A., Stage, M., Wooden, J., Constantz, B. R., Dunbar, R. B., Owen, A., Grumet, N., Bacon, C. R., and Chamberlain, C. P.: Monthly Strontium/Calcium oscillations in symbiotic coral aragonite: Biological effects limiting the precision of the paleotemperature proxy, Geophys. Res. Lett., 30, https://doi.org/10.1029/2002GL016864, 2003.

Meyers, S. R.: Seeing red in cyclic stratigraphy: Spectral noise estimation for astrochronology, Paleoceanography, 27, 2012.

Meyers, S. R.: Astrochron: An R package for astrochronology, http://cran.r-project.org/package=astrochron, 2014.

Mohammed, T. A. A., Mohamed, M. H., Zamzamy, R. M., and Mahmoud, M. A. M.: Growth rates of the giant clam Tridacna maxima (Röding, 1798) reared in cages in the Egyptian Red Sea, Egypt. J. Aquat. Res., 45, 67–73, https://doi.org/10.1016/j.ejar.2019.02.003, 2019.

Munro, J. L.: Estimation of the parameters of the von Bertalanffy growth equation from recapture data at variable time intervals, ICES J. Mar. Sci., 40, 199–200, https://doi.org/10.1093/icesjms/40.2.199, 1982.

Nassar, M. Z., Mohamed, H. R., Khiray, H. M., and Rashedy, S. H.: Seasonal fluctuations of phytoplankton community and physico-chemical parameters of the north western part of the Red Sea, Egypt, Egypt. J. Aquat. Res., 40, 395–403, https://doi.org/10.1016/j.ejar.2014.11.002, 2014.

Nedoncelle, K., Lartaud, F., de Rafelis, M., Boulila, S., and Le Bris, N.: A new method for high-resolution bivalve growth rate studies in hydrothermal environments, Mar. Biol., 160, 1427–1439, https://doi.org/10.1007/s00227-013-2195-7, 2013.

Onuma, N., Masuda, F., Hirano, M., and Wada, K.: Crystal structure control on trace element partition in molluscan shell formation, Geochem. J., 13, 187–189, 1979.

Pandolfi, J. M. and Kiessling, W.: Gaining insights from past reefs to inform understanding of coral reef response to global climate change, Curr. Opin. Environ. Sustain., 7, 52–58, https://doi.org/10.1016/j.cosust.2013.11.020, 2014.

Pannella, G.: Tidal growth patterns in recent and fossil mollusc bivalve shells: a tool for the reconstruction of paleotides, Naturwissenschaften, 63, 539–543, 1976.

Petersen, S. V., Tabor, C. R., Lohmann, K. C., Poulsen, C. J., Meyer, K. W., Carpenter, S. J., Erickson, J. M., Matsunaga, K. K., Smith, S. Y., and Sheldon, N. D.: Temperature and salinity of the Late Cretaceous western interior seaway, Geology, 44, 903–906, 2016.

Poitevin, P., Chauvaud, L., Pécheyran, C., Lazure, P., Jolivet, A., and Thébault, J.: Does trace element composition of bivalve shells record utra-high frequency environmental variations?, Mar. Environ. Res., 158, 104943, https://doi.org/10.1016/j.marenvres.2020.104943, 2020.

Polsenaere, P., Deflandre, B., Thouzeau, G., Rigaud, S., Cox, T., Amice, E., Bec, T. L., Bihannic, I., and Maire, O.: Comparison of benthic oxygen exchange measured by aquatic Eddy Covariance and Benthic Chambers in two contrasting coastal biotopes (Bay of Brest, France), Reg. Stud. Mar. Sci., 43, 101668, https://doi.org/10.1016/j.rsma.2021.101668, 2021.

Popov, S. V.: Formation of bivalve shells and their microstructure, Paleontol. J., 48, 1519–1531, https://doi.org/10.1134/S003103011414010X, 2014.

R Core Team: R: A language and environment for statistical computing. R Foundation for Statistical Computing, 2013.

Richard, M.: Analyse de la composition élémentaire de Pecten maximus par HR-ICP-MS Element 2: développements méthodologiques et interprétations écologiques., PhD Thesis, Université de Bretagne occidentale-Brest, 2009.

Richardson, C. A., Crisp, D. J., Runham, N. W., and Gruffydd, L. D.: The use of tidal growth bands in the shell of Cerastoderma edule to measure seasonal growth rates under cool temperate and sub-arctic conditions, J. Mar. Biol. Assoc. U. K., 60, 977–989, https://doi.org/10.1017/S002531540004203X, 1980.

Richter, C., Roa-Quiaoit, H., Jantzen, C., Al-Zibdah, M., and Kochzius, M.: Collapse of a new living species of giant clam in the Red Sea, Curr. Biol., 18, 1349–1354, 2008.

Roa-Quiaoit, H.: Ecology and culture of giant clams (Tridacnidae) in the Jordanian sector of the Gulf of Aqaba, Red Sea, Httpelibsuubuni-BremendedissdocsE-Diss1340PHDROAQpdf, 2005.

Roberts, E. M., Bowers, D. G., and Davies, A. J.: Tidal modulation of seabed light and its implications for benthic algae, Limnol. Oceanogr., 63, 91–106, https://doi.org/10.1002/lno.10616, 2018.

Robson, A. A., Chauvaud, L., Wilson, R. P., and Halsey, L. G.: Small actions, big costs: the behavioural energetics of a commercially important invertebrate, J. R. Soc. Interface, 9, 1486–1498, https://doi.org/10.1098/rsif.2011.0713, 2012.

Rodland, D. L., Schöne, B. R., Helama, S., Nielsen, J. K., and Baier, S.: A clockwork mollusc: Ultradian rhythms in bivalve activity revealed by digital photography, J. Exp. Mar. Biol. Ecol., 334, 316–323, https://doi.org/10.1016/j.jembe.2006.02.012, 2006.

Sano, Y., Kobayashi, S., Shirai, K., Takahata, N., Matsumoto, K., Watanabe, T., Sowa, K., and Iwai, K.: Past daily light cycle recorded in the strontium/calcium ratios of giant clam shells, Nat. Commun., 3, 761, https://doi.org/10.1038/ncomms1763, 2012.

Sather, W. A. and McCleskey, E. W.: Permeation and selectivity in calcium channels, Annu. Rev. Physiol., 65, 133–159, 2003.

Savitzky, A. and Golay, M. J.: Smoothing and differentiation of data by simplified least squares procedures., Anal. Chem., 36, 1627–1639, 1964.

Schöne, B. R. and Giere, O.: Growth increments and stable isotope variation in shells of the deep-sea hydrothermal vent bivalve mollusk Bathymodiolus brevior from the North Fiji Basin, Pacific Ocean, Deep Sea Res. Part Oceanogr. Res. Pap., 52, 1896–1910, 2005.

Schöne, B. R. and Gillikin, D. P.: Unraveling environmental histories from skeletal diaries — Advances in sclerochronology, Palaeogeogr. Palaeoclimatol. Palaeoecol., 373, 1–5, https://doi.org/10.1016/j.palaeo.2012.11.026, 2013.

Schöne, B. R., Castro, A. D. F., Fiebig, J., Houk, S. D., Oschmann, W., and Kröncke, I.: Sea surface water temperatures over the period 1884–1983 reconstructed from oxygen isotope ratios of a bivalve mollusk shell (Arctica islandica, southern North Sea), Palaeogeogr. Palaeoclimatol. Palaeoecol., 212, 215–232, 2004.

Schöne, B. R., Fiebig, J., Pfeiffer, M., Gleβ, R., Hickson, J., Johnson, A. L., Dreyer, W., and Oschmann, W.: Climate records from a bivalved Methuselah (Arctica islandica, Mollusca; Iceland), Palaeogeogr. Palaeoclimatol. Palaeoecol., 228, 130–148, 2005a.

Schöne, B. R., Houk, S. D., Castro, A. D. F., Fiebig, J., Oschmann, W., Kröncke, I., Dreyer, W., and Gosselck, F.: Daily growth rates in shells of Arctica islandica: assessing sub-seasonal environmental controls on a long-lived bivalve mollusk, Palaios, 20, 78–92, 2005b.

Schöne, B. R., Dunca, E., Fiebig, J., and Pfeiffer, M.: Mutvei's solution: An ideal agent for resolving microgrowth structures of biogenic carbonates, Palaeogeogr. Palaeoclimatol. Palaeoecol., 228, 149–166, https://doi.org/10.1016/j.palaeo.2005.03.054, 2005c.

Schöne, B. R., Zhang, Z., Jacob, D., Gillikin, D. P., Tütken, T., Garbe-Schönberg, D., and SOLDATI, A.: Effect of organic matrices on the determination of the trace element chemistry (Mg, Sr, Mg/Ca, Sr/Ca) of aragonitic bivalve shells (Arctica islandica)—Comparison of ICP-OES and LA-ICP-MS data, Geochem. J., 44, 23–37, 2010.

Schwartzmann, C., Durrieu, G., Sow, M., Ciret, P., Lazareth, C. E., and Massabuau, J.-C.: In situ giant clam growth rate behavior in relation to temperature: A one-year coupled study of high-frequency noninvasive valvometry and sclerochronology, Limnol. Oceanogr., 56, 1940–1951, https://doi.org/10.4319/lo.2011.56.5.1940, 2011.

Service Hydrographique et Océanographique de la Marine - Géoportail: https://www.geoportail.gouv.fr/, last access: 28 June 2022.

Sinclair, D. J., Kinsley, L. P. J., and McCulloch, M. T.: High resolution analysis of trace elements in corals by laser ablation ICP-MS, Geochim. Cosmochim. Acta, 62, 1889–1901, https://doi.org/10.1016/S0016-7037(98)00112-4, 1998.

Soldati, A. L., Jacob, D. E., Glatzel, P., Swarbrick, J. C., and Geck, J.: Element substitution by living organisms: the case of manganese in mollusc shell aragonite, Sci. Rep., 6, 1–9, 2016.

Soo, P. and Todd, P. A.: The behaviour of giant clams (Bivalvia: Cardiidae: Tridacninae), Mar. Biol., 161, 2699–2717, https://doi.org/10.1007/s00227-014-2545-0, 2014.

Surge, D., Lohmann, K. C., and Dettman, D. L.: Controls on isotopic chemistry of the American oyster, Crassostrea virginica: implications for growth patterns, Palaeogeogr. Palaeoclimatol. Palaeoecol., 172, 283–296, 2001.

Takesue, R. K., Bacon, C. R., and Thompson, J. K.: Influences of organic matter and calcification rate on trace elements in aragonitic estuarine bivalve shells, Geochim. Cosmochim. Acta, 72, 5431–5445, 2008.

Tanaka, K., Okaniwa, N., Miyaji, T., Murakami-Sugihara, N., Zhao, L., Tanabe, K., Schöne, B. R., and Shirai, K.: Microscale magnesium distribution in shell of the Mediterranean mussel Mytilus galloprovincialis: An example of multiple factors controlling Mg/Ca in biogenic calcite, Chem. Geol., 511, 521–532, https://doi.org/10.1016/j.chemgeo.2018.10.025, 2019.

Taylor, J. D. and Layman, M.: The mechanical properties of bivalve (Mollusca) shell structures, Palaeontology, 15, 73–87, 1972.

Thébault, J., Chauvaud, L., L'Helguen, S., Clavier, J., Barats, A., Jacquet, Sé., PÉcheyran, C., and Amouroux, D.: Barium and molybdenum records in bivalve shells: Geochemical proxies for phytoplankton dynamics in coastal environments?, Limnol. Oceanogr., 54, 1002–1014, https://doi.org/10.4319/lo.2009.54.3.1002, 2009.

Thébault, J., Jolivet, A., Waeles, M., Tabouret, H., Sabarot, S., Pécheyran, C., Leynaert, A., Jochum, K. P., Schöne, B. R., Fröhlich, L., Siebert, V., Amice, E., and Chauvaud, L.: Scallop shells as geochemical archives of phytoplankton-related ecological processes in a temperate coastal ecosystem, Limnol. Oceanogr., 67, 187–202, https://doi.org/10.1002/lno.11985, 2022.

Thomson, D. J.: Spectrum estimation and harmonic analysis, Proc. IEEE, 70, 1055–1096, 1982.

Tierney, J. E., Poulsen, C. J., Montañez, I. P., Bhattacharya, T., Feng, R., Ford, H. L., Hönisch, B., Inglis, G. N., Petersen, S. V., Sagoo, N., Tabor, C. R., Thirumalai, K., Zhu, J., Burls, N. J., Foster, G. L., Goddéris, Y., Huber, B. T., Ivany, L. C., Turner, S. K., Lunt, D. J., McElwain, J. C., Mills, B. J. W., Otto-Bliesner, B. L., Ridgwell, A., and Zhang, Y. G.: Past climates inform our future, Science, 370, https://doi.org/10.1126/science.aay3701, 2020.

Tran, D., Nadau, A., Durrieu, G., Ciret, P., Parisot, J.-P., and Massabuau, J.-C.: Field chronobiology of a molluscan bivalve: how the moon and sun cycles interact to drive oyster activity rhythms, Chronobiol. Int., 28, 307–317, 2011.

Tran, D., Perrigault, M., Ciret, P., and Payton, L.: Bivalve mollusc circadian clock genes can run at tidal frequency, Proc. R. Soc. B Biol. Sci., 287, 20192440, https://doi.org/10.1098/rspb.2019.2440, 2020.

Vander Putten, E., Dehairs, F., Keppens, E., and Baeyens, W.: High resolution distribution of trace elements in the calcite shell layer of modern Mytilus edulis: Environmental and biological controls, Geochim. Cosmochim. Acta, 64, 997–1011, 2000.

Vermeij, G. J.: The evolution of molluscan photosymbioses: a critical appraisal, Biol. J. Linn. Soc., 109, 497–511, 2013.

Von Bertalanffy, L.: Quantitative laws in metabolism and growth, Q. Rev. Biol., 32, 217–231, 1957.

Warter, V. and Müller, W.: Daily growth and tidal rhythms in Miocene and modern giant clams revealed via ultra-high resolution LA-ICPMS analysis—A novel methodological approach towards improved sclerochemistry, Palaeogeogr. Palaeoclimatol. Palaeoecol., 465, 362–375, 2017.

Warter, V., MÜLLER, W., WESSELINGH, F. P., TODD, J. A., and RENEMA, W.: LATE MIOCENE SEASONAL TO SUBDECADAL CLIMATE VARIABILITY IN THE INDO-WEST PACIFIC (EAST KALIMANTAN, INDONESIA) PRESERVED IN GIANT CLAMS, PALAIOS, 30, 66–82, https://doi.org/10.2110/palo.2013.061, 2015.

Warter, V., Erez, J., and Müller, W.: Environmental and physiological controls on daily trace element incorporation in Tridacna crocea from combined laboratory culturing and ultra-high resolution LA-ICP-MS analysis, Palaeogeogr. Palaeoclimatol. Palaeoecol., 496, 32–47, https://doi.org/10.1016/j.palaeo.2017.12.038, 2018.

Wassenburg, J. A., Scholz, D., Jochum, K. P., Cheng, H., Oster, J., Immenhauser, A., Richter, D. K., Häger, T., Jamieson, R. A., Baldini, J. U. L., Hoffmann, D., and Breitenbach, S. F. M.: Determination of aragonite trace element distribution coefficients from speleothem calcite–aragonite transitions, Geochim. Cosmochim. Acta, 190, 347–367, https://doi.org/10.1016/j.gca.2016.06.036, 2016.

Wichern, N. M. A., de Winter, N. J., Johnson, A. L. A., Goolaerts, S., Wesselingh, F., Hamers, M. F., Kaskes, P., Claeys, P., and Ziegler, M.: The fossil bivalve Angulus benedeni benedeni: a potential seasonally resolved stable isotope-based climate archive to investigate Pliocene temperatures in the southern North Sea basin, EGUsphere, 1–53, https://doi.org/10.5194/egusphere-2022-951, 2022.

Wilson, S. A., Koenig, A. E., and Orklid, R.: Development of microanalytical reference material (MACS-3) for LA-ICP-MS analysis of carbonate samples, Geochim. Cosmochim. Acta Suppl., 72, A1025, 2008.

de Winter, N. J. and Claeys, P.: Micro X-ray fluorescence (μXRF) line scanning on Cretaceous rudist bivalves: A new method for reproducible trace element profiles in bivalve calcite, Sedimentology, 64, 231–251, https://doi.org/10.1111/sed.12299, 2017.

de Winter, N. J., Goderis, S., Dehairs, F., Jagt, J. W., Fraaije, R. H., Van Malderen, S. J., Vanhaecke, F., and Claeys, P.: Tropical seasonality in the late Campanian (late Cretaceous): Comparison between multiproxy records from three bivalve taxa from Oman, Palaeogeogr. Palaeoclimatol. Palaeoecol., 485, 740–760, 2017.

de Winter, N. J., Vellekoop, J., Vorsselmans, R., Golreihan, A., Soete, J., Petersen, S. V., Meyer, K. W., Casadio, S., Speijer, R. P., and Claeys, P.: An assessment of latest Cretaceous Pycnodonte vesicularis (Lamarck, 1806) shells as records for palaeoseasonality: a multi-proxy investigation, Clim. Past, 14, 725–749, 2018.

de Winter, N. J., Goderis, S., Malderen, S. J. M. V., Sinnesael, M., Vansteenberge, S., Snoeck, C., Belza, J., Vanhaecke, F., and Claeys, P.: Subdaily-Scale Chemical Variability in a Torreites Sanchezi Rudist Shell: Implications for Rudist Paleobiology and the Cretaceous Day-Night Cycle, Paleoceanogr. Paleoclimatology, 35, e2019PA003723, https://doi.org/10.1029/2019PA003723, 2020.

de Winter, N. J., Müller, I. A., Kocken, I. J., Thibault, N., Ullmann, C. V., Farnsworth, A., Lunt, D. J., Claeys, P., and Ziegler, M.: Absolute seasonal temperature estimates from clumped isotopes in bivalve shells

suggest warm and variable greenhouse climate, Commun. Earth Environ., 2, 1–8, https://doi.org/10.1038/s43247-021-00193-9, 2021a.

de Winter, N. J., Agterhuis, T., and Ziegler, M.: Optimizing sampling strategies in high-resolution paleoclimate records, Clim. Past, 17, 1315–1340, https://doi.org/10.5194/cp-17-1315-2021, 2021b.

de Winter, N. J., Witbaard, R., Kocken, I. J., Müller, I. A., Guo, J., Goudsmit, B., and Ziegler, M.: Temperature Dependence of Clumped Isotopes (Δ47) in Aragonite, Geophys. Res. Lett., 49, e2022GL099479, https://doi.org/10.1029/2022GL099479, 2022.

Winter, N. J. de, Sikkeleras, S. van, Goudsmit-Hazevoort, B., Boer, W., Nooijer, L. de, Reichart, G.-J., Claeys, P., and Witbaard, R.: Tracing timing of growth in cultured mollusks using strontium spiking, 2022.

Wisshak, M., Correa, M. L., Gofas, S., Salas, C., Taviani, M., Jakobsen, J., and Freiwald, A.: Shell architecture, element composition, and stable isotope signature of the giant deep-sea oyster Neopycnodonte zibrowii sp. n. from the NE Atlantic, Deep Sea Res. Part Oceanogr. Res. Pap., 56, 374–407, 2009.

Witbaard, R., Jenness, M. I., Van Der Borg, K., and Ganssen, G.: Verification of annual growth increments in Arctica islandica L. from the North Sea by means of oxygen and carbon isotopes, Neth. J. Sea Res., 33, 91–101, https://doi.org/10.1016/0077-7579(94)90054-X, 1994.

Xing, Q., Zhang, L., Li, Y., Zhu, X., Li, Y., Guo, H., Bao, Z., and Wang, S.: Development of Novel Cardiac Indices and Assessment of Factors Affecting Cardiac Activity in a Bivalve Mollusc Chlamys farreri, Front. Physiol., 10, 2019.

Yan, H., Shao, D., Wang, Y., and Sun, L.: Sr/Ca profile of long-lived Tridacna gigas bivalves from South China Sea: A new high-resolution SST proxy, Geochim. Cosmochim. Acta, 112, 52–65, https://doi.org/10.1016/j.gca.2013.03.007, 2013.

Yan, H., Liu, C., An, Z., Yang, W., Yang, Y., Huang, P., Qiu, S., Zhou, P., Zhao, N., Fei, H., Ma, X., Shi, G., Dodson, J., Hao, J., Yu, K., Wei, G., Yang, Y., Jin, Z., and Zhou, W.: Extreme weather events recorded by daily to hourly resolution biogeochemical proxies of marine giant clam shells, Proc. Natl. Acad. Sci., 117, 7038–7043, https://doi.org/10.1073/pnas.1916784117, 2020.

Yoshimura, T., Suzuki, A., Tamenori, Y., and Kawahata, H.: Micro-X-ray fluorescence-based comparison of skeletal structure and P, Mg, Sr, O and Fe in a fossil of the cold-water coral Desmophyllum sp., NW Pacific, Geo-Mar. Lett., 34, 1–9, 2014.

Zhao, L., Schöne, B. R., and Mertz-Kraus, R.: Controls on strontium and barium incorporation into freshwater bivalve shells (Corbicula fluminea), Palaeogeogr. Palaeoclimatol. Palaeoecol., 465, 386–394, https://doi.org/10.1016/j.palaeo.2015.11.040, 2017.